Gcn5 – mTORC1 – TFEB signalling axis mediated control of autophagy regulates *Drosophila* blood cell homeostasis

Arjun Aji Reeja[1,3*], Mincy Kunjumon[1,2*], Suraj Math[1,4], Laxmi Kata[1] and Rohan Jayant Khadilkar[1,2 ±]

1. Stem Cell and Tissue Homeostasis laboratory, Advanced Centre for Treatment, Research and Education in Cancer (ACTREC), Tata Memorial Centre, Kharghar, Navi Mumbai, Maharashtra, 410210, India.
2. Homi Bhabha National Institute, Training School Complex, Anushakti Nagar, Mumbai, 400085, India.
3. Champalimaud Research, Champalimaud Foundation, Avenida Brasília, 1400-038 Lisboa - Portugal
4. Center for Genomic Medicine, Massachusetts General Hospital, 185 Cambridge Street, Boston, MA 02114, USA

± Corresponding author - email: rkhadilkar@actrec.gov.in

* indicates equal contribution

Keywords: Gcn5, Autophagy, Hematopoiesis, Homeostasis, *Drosophila*

Running title: Gcn5-mTORC1-TFEB in *Drosophila* blood cell homeostasis

Abstract:

Blood progenitors are regulated by a variety of systemic and nutritional cues from their environment. In the *Drosophila* lymph gland (LG), the Posterior Signalling Center (PSC) acts as a stem cell niche striking a balance between progenitors and differentiated blood cells. Blood progenitors maintain homeostasis by fine tuning intrinsic and extrinsic cues.. Autophagy is one such cellular process that maintains homeostasis by removing unnecessary or dysfunctional cell components through autophagic degradation and recycling. Here, using genetic perturbation analysis we show that autophagy plays a critical role in regulating LG blood cell homeostasis. General control non-derepressible 5 (Gcn5), a histone acetyltransferase is expressed in the primary LG lobe and modulation of Gcn5 levels perturbs LG homeostasis. Our results demonstrate thatGcn5 through its known non-histone acetylation target, TFEB controls autophagic flux in the hemocytes.. Additionally, we show that modulation of mTORC1 activity can perturb hematopoiesis. Our results indicate that Gcn5 acts as a nutrient sensor and modulation of mTORC1 activity regulates Gcn5. Chemical intervention shows that mTORC1 over-rides the effect exerted by Gcn5 in regulating LG hematopoiesis. Taken together, our findings indicate that Gcn5 – mTORC1 – TFEB signaling axis mediated control of autophagy is required for maintaining blood cell homeostasis in *Drosophila.*

Introduction:

Drosophila hematopoiesis occurs in two different waves: the first wave occurs in the embryonic stages in the procephalic mesoderm giving rise to both circulating and sessile pool of hemocytes. While the second wave of definitive hematopoiesis begins in the dorsal mesoderm, giving rise to the lymph gland (LG), the larval hematopoietic organ [1,2]. The larval LG can be divided into functionally distinct regions: the Posterior Signaling Center (PSC), which acts as the stem cell niche producing signals that are not only required for maintaining the prohemocytes but also for priming them towards differentiation. The Medullary Zone (MZ) is made up of prohemocytes (hematopoietic progenitors) that are capable of differentiating into three differentiated blood cell types namely plasmatocytes, crystal cells and lamellocytes. The Cortical Zone (CZ) houses the differentiated blood cell population [3]. Single cell sequencing efforts have identified heterogeneity amongst the developing hemocytes in the LG and have discovered previously unreported hemocyte types like adipohemocytes, stem-like prohemocytes, intermediate prohemocytes, early lamellocytes suggesting that there is a lot of heterogeneity in the cell types present within the LG for example the subsets identified within the progenitors: core, distal and intermediate [4,5]. These recent single cell sequencing based studies show that the LG is a complex organ with multiple hemocyte types and consists of an intricate array of signals that regulate them [4,6].

The cellular fate of prohemocytes in the medullary zone is intricately controlled by a set of extrinsic and intrinsic signals. Multiple signaling pathways like the JAK/STAT, Hedgehog, Wingless, Dpp have been reported to play an important role in prohemocyte maintenance [7–15]. Stem cell and tissue homeostasis is closely linked to the nutritional status of the organism. There is increasing evidence indicating the involvement of nutrient signals in stem/progenitor cell fate [16–19]. *Drosophila* hematopoietic progenitors are capable of sensing systemic and nutritional cues. Starvation has been shown to alter the homeostatic balance in the LG mimicking an inflammatory response like scenario causing excessive differentiation of blood cells [20]. Also, perturbation of key nutrient sensing pathways like the IIS/Tor signaling has been shown to affect niche numbers as well as progenitor differentiation [21]. More specifically TORC1 has been shown to play an important role during *Drosophila* hematopoiesis. TORC1 activity has been shown to promote the proliferation and expansion of progenitor pools[22]. Knocking down TOR signaling components in the *Drosophila* hematopoietic niche has shown to cause a cell autonomous reduction in the niche numbers. Activation of Tor signaling on the other hand results in excess progenitor differentiation. This shows that a fine tuning of the nutrient sensing pathways is important for progenitor maintenance [23]. Autophagy a cell intrinsic process is also known to be responsive to nutritional status and stress. Autophagy ensures cellular homeostasis by removing intracellular waste material, replaces old and damaged organelles and sustains cell survival during nutrient deprived conditions [24,25]. mTOR (molecular target of rapamycin) is an important regulator of autophagy. mTORC1 inhibits autophagy in nutrient replete conditions by targeting either initiation, expansion or termination of autophagy [26]. Several studies indicate that autophagy is essential for the maintenance of hematopoietic stem cells [27–29]. There have been several reports that investigate the role of key autophagy genes in hematopoiesis and show that mice lacking functional autophagy genes like Atg7, Atg12 or FIP200 lead to an exhaustion of the HSC pool especially long-term HSCs thus showing that autophagy is critical for HSC maintenance [28,30,31]. Furthermore, HSCs

lacking Atg12 displayed phenotypes similar to aged HSCs viz. increased mitochondrial content, heightened metabolic activity, myeloid differentiation bias [27]. Similarly, autophagy genes are shown to affect *Drosophila* hematopoiesis, it has been shown that Atg6 mutants show an enlarged LG and possess elevated blood cell numbers [32]. Perturbing autophagy by knocking down Atg1 affected hemocyte spreading and recruitment to wound site[33]. Inhibiting Atg2, induced melanotic nodule formation, impaired the ability to respond to bacterial infection by altering the expression of AMP (Anti -Microbial peptides) genes as well as disrupting phagocytosis [34].Mis-regulation of the autophagic process can lead to leukemogenesis[35]. Though the role of autophagy has been explored in mammalian hematopoiesis, its role and mechanisms it controls during *Drosophila* hematopoiesis is unexplored. There are various nutrient sensors that can sense systemic nutrient signals and regulate cellular processes like autophagy. In this study, we report that General control non-depressible 5 (GCN5), a histone acetyltransferase, regulates the process of autophagy during hematopoiesis through its non-histone acetylation target, TFEB.

General control non-depressible 5 (GCN5) is the first nuclear histone acetyltransferase (HAT) to be identified with function in transcriptional regulation by serving as a key subunit in transcriptional coactivator complexes like SAGA (Spt-Ada-Gcn5-acetyltransferase) and ATAC (Ada-2A-containing) [36–38]. The transfer of acetyl group to the lysine residues of histones mediates HAT activity[39] . The primary acetylation site of Gcn5 is lysine 14 of Histone 3 (H3K14) whereas other lysine residues of Histone 3 like H3K9, H3K18, H3K23, H3K27 are also found to be acetylated by Gcn5[40] . Recent studies reported the additional role of Gcn5 in histone succinylation as well as crotonylation[41–43]. Gcn5 has important functions in the extension of lifespan[44] , metabolism [45], cellular differentiation[46] , cell proliferation and growth[47] , neuronal apoptosis[48] and DNA damage response [49]. GCN5 acts as an oncoprotein in cancer and its inhibition can rescue cancer phenotypes in various cancers namely hepatocellular carcinoma, glioma, non-small cell lung carcinoma[50–52] . Gcn5 is over-expressed in Acute Myeloid Leukemia (AML) and is needed for the survival of AML cell lines [53]. Aberrant acetylation of H3K9 by GCN5 leads to all-trans Retinoic acid (ATRA) resistance in non-APL AML, thereby preventing the maturation of myeloid blasts and maintaining them in a leukemic state[54] . GCN5 plays a role in drug resistance in the leukemic early drug-resistant population (EDRP) where it interacts with ATM thereby recruiting ATM to the DNA damage site [55]. With an evolutionary well conserved structure and function, the significance of Gcn5 in different cellular processes can be studied using a variety of model organisms[42] . *Drosophila* has only one homolog of Gcn5 (dGCN5), hence making it an efficient model to study the functions of Gcn5 [56]. In *Drosophila*, loss of Gcn5 function affects developmental processes like oogenesis, metamorphosis[57] . Gcn5 plays an important role in germline stem cell maintenance[58] . Other than the developmental processes, Gcn5 was shown to regulate a cellular process like autophagy by targeting TFEB, a non-histone acetylation target of Gcn5 that activates genes responsible for autophagosomal and lysosome biogenesis [59]. mTORC1 regulates autophagy not only through the initiator kinase, Ulk1 arm but also through inhibitory phosphorylation of TFEB [60]. In the context of hematopoiesis, Gcn5 is necessary for T-cell development and function, and deletion of Gcn5 could affect the development of immune cells in vertebrates[46] . Gcn5 expression increases during the differentiation phase of human CD34 cells indicating an important role of Gcn5 in erythroid differentiation[61] . Although there are studies demonstrating the role of Gcn5 in leukemogenesis there is paucity of information on its role in physiological hematopoiesis. In *Drosophila*, a study reported that loss of a HAT like Gcn5 or Chameau phenocopies the differentiation defect seen upon loss of function of molecules regulating

fatty acid oxidation[62] . There are no other studies that have explored the role of Gcn5 during normal hematopoiesis in *Drosophila*.

Here, we show that Gcn5 plays an essential role in regulating blood cell homeostasis in the *Drosophila* LG. Analysis of *gcn5* mutants, cellular subset specific modulation of Gcn5 levels in the LG and by utilizing structure function approaches in the LG, we show that Gcn5 function is important for developmental hematopoiesis. Our results demonstrate that modulation of Gcn5 levels alter blood cell homeostasis via its regulation of autophagy. We show that autophagy plays a critical role in the LG by controlling blood cell differentiation. Gcn5 acts as a nutrient sensor and negatively regulates autophagy through its non-histone acetylation target, TFEB. Additionally, our findings indicate that modulation of mTORC1 activity can regulate Gcn5 levels and perturb LG hematopoiesis. mTORC1 over-rides the effect exerted by Gcn5 in regulating LG hematopoiesis. Taken together, we suggest that the Gcn5 – mTORC1 – TFEB signaling axis mediated control of autophagy is required for maintaining blood cell homeostasis in *Drosophila*.

Results:

Gcn5 is expressed in all the cellular subsets of the primary LG lobe

Gcn5 has been previously reported to be overexpressed in acute myeloid leukemias (AML) and is required for the survival of AML cells [53–55]. In *Drosophila*, Gcn5 has been shown to play an important role during metamorphosis and in the maintenance of germline stem cells[57,58] . However, its role in *Drosophila* hematopoiesis is unknown. We first set out to understand the expression of Gcn5 in the *Drosophila* LG where the primary lobe is the main site of active hematopoiesis. The primary lobe consists of various developmental zones housing different cell populations with identifiable markers (Fig. 1A, B). Gcn5 expression analysis shows that Gcn5 is expressed in all cellular subpopulations of the primary LG lobe including the Posterior Signalling Center (PSC, Fig 1C-C', E-E''), Dome positive medullary zone (MZ) progenitors and Dome negative hemocytes in the LG (Fig 1D-D', F-F'). Gcn5 is also expressed in the posterior LG lobes (Fig. S5E-F).

Whole animal *gcn5* mutants show defective blood cell homeostasis

Since Gcn5 is expressed in all the cellular subpopulations of the LG, we were interested to know if hematopoiesis gets affected in the whole animal *gcn5* mutants. We first characterized the hematopoietic phenotypes of the *gcn5* null allele, *gcn5[E333st]* and the hypomorphic allele, *gcn5[C137Y]* in heterozygous conditions. We observed that the Antennapedia positive PSC cell numbers were not affected in the *gcn5[C137Y/+]* or *gcn5[E333st/+]* heterozygous mutants compared to wildtype (Fig S1A-D). Excessive differentiation of P1 (NimRodC1) positive plasmatocytes was observed in the *gcn5[E333st/+]* mutant whereas no significant change was seen in the *gcn5[C137Y/+]* mutant compared to wildtype (Fig S1E-H). In contrast, a significant increase in Hindsight positive Crystal cell differentiation and gamma-H2Ax positive DNA damage foci were observed in both *gcn5[C137Y/+]* and *gcn5[E333st/+]* mutants, compared to wildtype (Fig S1I-P). We assessed the impact of Gcn5 perturbation on DNA damage accumulation due to its known role in regulating DNA damage repair [49,63,64]. We then combined these alleles in homozygous and trans-heterozygous combinations. The *gcn5 [C137Y]* hypomorphic allele and the null allele *gcn5 [E333st]* null allele were combined which yielded viable homozygous larvae whose LG hematopoietic phenotypes were studied. We also generated *gcn5 [C137Y]/gcn5 [E333st]* transheterozygotes in order to study the hematopoietic phenotypes of the *gcn5* mutants. Our analysis reveals that the PSC cell numbers were reduced in the *gcn5[E333st/C137Y]* transheterozygous mutant as well as the *gcn5[E333st/ E333st]* mutant whereas no change was observed in the *gcn5[C137Y/C137Y]* homozygous mutant, compared to wildtype (Fig 2A-E). Plasmatocyte differentiation significantly increased in the *gcn5[C137Y/C137Y]* and *gcn5[E333st/ E333st]* homozygous mutants, whereas no significant change was observed in *gcn5[E333st/C137Y]* transheterozygous mutant compared to wildtype (Fig 2F-J). A significant increase in crystal cell differentiation and DNA damage was observed among all the three mutants *gcn5[C137Y/C137Y]*, *gcn5[E333st/C137Y]* and *gcn5[E333st/ E333st]* respectively, compared to wildtype (Fig 2K-T). Since these are all whole animal mutants of Gcn5, there could be a number of systemic signals that could contribute to these changes in hematopoiesis as the LG is very sensitive to systemic signals and responds rapidly. Further characterization of systemic signals and signaling mechanisms that are causing these aberrations in hematopoesis needs to be done,

LG cellular subset-specific modulation of Gcn5 levels results in aberrant hematopoiesis

The observations from *gcn5* mutants led us to question if the modulation of Gcn5 levels in different cellular populations of the LG affects hematopoiesis. In order to modulate Gcn5 levels, we have depleted or over-expressed Gcn5 in different cellular subsets of the LG. Validation of *Hml-Gal4* mediated knockdown or overexpression of Gcn5 has been done using immunostaining with Gcn5 antibody (Fig S2A-C'). The FLAG-tagged Gcn5 overexpression construct has been validated using the anti-FLAG tag antibody by immunostaining (Fig S2D-E').

Since the balance between the prohemocyte population and the differentiated blood cells is a determinant of the homeostasis conditions in the LG, we first depleted or overexpressed Gcn5 in the prohemocytes using *Dome-Gal4*. We observed that the PSC population remained unperturbed upon Gcn5 modulation in the prohemocytes as compared to wildtype (Fig 3A-C' and M). However, the Dome positive progenitor pool decreased significantly upon Gcn5 knockdown whereas overexpression resulted in no significant change (Fig 3N). Over-expression of Gcn5 using *Dome-Gal4* led to a significant increase in both plasmatocyte and crystal cell differentiation whereas knockdown of Gcn5 did not affect blood cell differentiation compared to wildtype (Fig 3D-I', O and P). An increase in DNA damage marked by Gamma H2Ax was observed upon knockdown of Gcn5 in the Dome population, whereas overexpression of Gcn5 did not lead to any change in DNA damage, as compared to wildtype (Fig 3J-L' and Q). This data shows that elevated levels of Gcn5 in the prohemocytes promotes differentiation whereas knockdown has no effect on differentiation which could be due to Gcn5 mediated differential regulation of signaling in progenitors. Since PSC is known to produce signals that are required not only for maintaining the prohemocytes but also for priming them towards differentiation we modulated Gcn5 levels in the PSC using *Collier-Gal4*. Over-expression of Gcn5 in the PSC led to a cell-autonomous increase in PSC cell numbers whereas knockdown had no change in the PSC population as compared to the wildtype (Fig S3A-C' and M). Plasmatocyte differentiation was reduced upon PSC- specific knockdown ofGcn5 whereas over-expression of Gcn5 did not affect plasmatocyte differentiation as compared to the wildtype (Fig S3D-F' and N). Crystal cell differentiation remained unaffected upon modulation of Gcn5 in the PSC as compared to wildtype (Fig S3G-I' and O). An increase in DNA damage was observed upon knockdown of Gcn5 in the PSC whereas over-expression did not lead to any change in DNA damage as compared to the wildtype (Fig S3J-L' and P). These results indicate that Gcn5 modulation in the PSC has non-autonomous effects in the LG which could be due to abrogation of signals that are produced by the PSC which needs further investigation. Gcn5 over-expression in PSC results in an increase in PSC numbers which could be due to modulation of local signals that are required for regulating niche cell numbers which needs to be tested. The non-autonomous increase in DNA damage in the LG upon Gcn5 depletion in the PSC could be due to production of inflammatory signals by PSC cells upon Gcn5 depletion resulting in DNA damage which needs further investigation.

Since over-expression of Gcn5 in the prohemocyte population resulted in an increase in blood cell differentiation we wanted to understand if perturbing Gcn5 levels in the differentiated blood cell population using Hmldelta-Gal4 alters blood cell differentiation cell-autonomously. A non-cell-

autonomous increase in the PSC population was observed upon knockdown or over-expression of Gcn5 using Hmldelta-Gal4 as compared to wildtype (Fig S4A-C' and M). Plasmatocyte differentiation remained unaffected upon modulation of Gcn5 levels in the Hmldelta positive population compared to wildtype (Fig S4D-F' and N), whereas a cell-autonomous increase in the crystal cell differentiation was observed upon overexpression of Gcn5 in the Hmldelta positive population whereas knockdown of Gcn5 did not affect the crystal cell differentiation compared to wildtype (Fig S4G-I' and O). This data clearly indicates that Gcn5 has a cell autonomous role in regulating crystal cell differentiation. Now, Gcn5 is expressed in the crystal cells (Fig S5A-B) and cell autonomous overexpression of Gcn5 using Lozenge- Gal4, a crystal cell specific driver resulted in a significant increase in cell autonomous crystal cell differentiation demonstrating a cell-autonomous role (Fig S5C-D and G). An increase in DNA damage was observed upon knockdown or over- expression of Gcn5 levels in the Hmldelta population, compared to wildtype (Fig S4J-L' and P). Overall, our analysis shows that modulation of Gcn5 levels in various sub-populations of the LG affects blood cell homeostasis.

Prohemocyte-specific expression of Gcn5 domain deletion constructs alters the hematopoietic program and results in increased DNA damage:

Gcn5 is an important component in the SAGA complex containing four different domains – the HAT, Pcaf, Ada, and Bromodomain (Fig.4A). We were further interested in investigating the functional role of each of the Gcn5 domains. In order to understand if any of the domain deletion constructs of Gcn5 perform a dominant negative function during hematopoiesis, we expressed Gcn5 lacking either the HAT, Pcaf, Ada or Bromodomain in the *Drosophila* prohemocytes using *tep4-Gal4*. A significant cell non-autonomous reduction in the PSC cell numbers was observed upon expression of Gcn5 domain deletion constructs in the prohemocyte population (Fig 4B-G). The tep4-GFP positive prohemocyte population was reduced upon expression of Bromo or Ada deletion constructs of Gcn5 using *tep4-Gal4*, whereas no change was observed upon expression of HAT or Pcaf domain deletion, compared to wildtype (Fig 4B'-F' and H). A significant decrease in plasmatocyte differentiation was seen upon expression of Pcaf domain deletion construct of Gcn5, whereas, expression of Bromo or Ada domain deletion constructs of Gcn5 led to a significant increase in plasmatocyte differentiation. On the other hand, expression of Gcn5 lacking HAT domain using *tep4-Gal4* did not have any significant change in plasmatocyte differentiation (Fig 4B"-F" and I). An increase in crystal cell differentiation was observed upon expression of HAT, Bromo, or Ada domain deletion of constructs of Gcn5, whereas expression of Gcn5 lacking Pcaf domain using *tep4-Gal4* did not affect crystal cell differentiation, compared to wildtype (Fig 4B"'-F"' and J). A significant increase in DNA damage was also observed upon expression of all domain deletion constructs of Gcn5 using *tep4-Gal4*, compared to wildtype (Fig S6A-F). These results indicate that various domains of Gcn5 play important roles during hematopoiesis which could be due to unique interactions facilitated by these domains. Expression of these domain deletion mutants in the wild type genetic background causes LG hematopoietic defects demonstrating dominant-negative effect of these domain deletion constructs which needs further investigation.

Autophagic flux in the *Drosophila* blood cells is negatively regulated by Gcn5

Increasing evidence suggests that Gcn5 can regulate gene expression programs linked to cellular metabolism [65]. Autophagy is a cellular process that is closely associated with cell metabolism regulation and intracellular quality control as it is involved in the turnover of undesired cellular components, damaged or dysfunctional organelles[24,25,66]. Autophagic flux is regulated by a number of molecules, one of them is Transcription Factor EB (TFEB) which is a known non- histone acetylation target of Gcn5. TFEB regulates expression of genes related to autophagosome formation and lysosome production which are critical for autophagy. Mammalian cell culture-based studies show that acetylation of TFEB by Gcn5 decreases TFEB transcriptional activity by disrupting its dimerization thereby affecting autophagy. Studies done in the *Drosophila* fat body indicate that Gcn5 negatively regulates formation of Atg8a puncta in starved conditions [59].

Hence, we sought to determine if Gcn5 regulates autophagic flux in *Drosophila* blood cells. We genetically modulated Gcn5 levels using a pan hemocyte driver, *Hml-Gal4* and probed the LG hemocytes for Ref(2)P/p62, an adaptor protein that is itself cleared during autophagy and Atg8 (homologue of human LC3). Our results indicate that there are no p62 puncta upon knockdown of Gcn5, whereas over-expression of Gcn5 led to an increase in p62 puncta, compared to wildtype (Fig 5A-C, D). On the contrary, immunostaining with Atg8 showed an increase in Atg8 puncta upon knockdown of Gcn5, whereas over-expression of Gcn5 leads to a significant reduction in the Atg8 puncta compared to wildtype (Fig 5A'-C', E). We also looked at the transcript levels of a panel of Atg genes involved during autophagy in the hemocytes upon over-expression of Gcn5 and our results indicate that Gcn5 over-expression using pan hemocyte driver, *Hml-Gal4* leads to a reduction in transcript levels of a panel of Atg genes in the hemocytes (Fig S7).

Genetic and chemical ablation of autophagy boosts blood cell differentiation in the primary LG lobe

Autophagy has been shown to regulate cellular homeostasis of all hematopoietic lineages in mammals[67]. Mis-regulation of autophagy in hematopoietic stem cells (HSC) leads to dysfunction and loss of HSCs with age[27]. Transcription factors that are considered to be master regulators of hematopoiesis have been shown to transcriptionally control autophagy related genes[29,68]. In *Drosophila*, Atg6 has been shown to play a role in multiple vesicle trafficking pathways and hematopoiesis[32].

Since we found that Gcn5 negatively regulates autophagy in *Drosophila* hemocytes, we asked the question whether key autophagy related genes regulate LG hematopoiesis. Since Gcn5 regulates autophagy via TFEB, a key regulator in autophagosome and lysosome biogenesis, we perturbed TFEB and several autophagy effector genes like Atg8a, Atg5, or Atg18a specifically in the *Drosophila* prohemocytes using tep4-Gal4. We observed that depleting TFEB or the autophagy effector genes in the tep population led to a drastic increase in both plasmatocyte and crystal cell differentiation in the LG along with a decrease in the tep4 positive prohemocyte index (Fig 6A-L, Fig S8M). Atg8 or TFEB knockdown did not affect the niche cell numbers, however Atg5 resulted in a significant increase in niche numbers whereas Atg18a knockdown resulted in a significant decrease. Depleting TFEB or the autophagy effector genes in the tep population led to a drastic increase in DNA damage. (Fig S8A-L). In addition to the genetic perturbation-based analysis,

chemical inhibition of autophagy by treating the larvae with autophagy inhibitor, chloroquine (CQ) for 16 hours resulted in a significant increase in blood cell differentiation in the LG (Fig 6M-R). We also validated the effect of CQ on autophagy and we find that there is an increase in p62 positive puncta and a decrease in Atg8 positive puncta per cell in the *Drosophila* LG upon CQ treatment for 16 hours (Fig S9A-F).

Chemical or genetic modulation of mTORC1 activity controls blood cell differentiation

mTOR signaling, specifically mTORC1 has been shown to play a significant role in hematopoietic lineage commitment in mice[69]. mTORC1 acts as a master regulator of autophagy and controls various steps of the autophagic process[26]. In nutrient replete conditions, mTORC1 phosphorylates ULK1, a key initiator kinase in autophagy thereby disrupting its interaction with AMPK and ULK1 activation by AMPK[70–73]. Similarly, mTORC1 phosphorylates TFEB in nutrient availability conditions at residues - S142 and S211 subjecting TFEB to localize in the cytoplasm rendering it inactive[74]. Since mTORC1 regulates critical nodal points that control autophagy we were curious to know if modulating mTORC1 activity alters blood cell homeostasis in the LG. We modulated mTORC1 activity by chemical modulation. We used 3BDO for mTOR activation and Rapamycin for mTOR inhibition. Upon treatment with the mTOR activator – 3BDO for 16 hours, a significant increase in both plasmatocyte and crystal cell differentiation was observed as compared to the control treatment (Fig 7A-F). Similarly, activation of mTOR genetically by overexpressing Rheb using tep4-Gal4 resulted in an increase in both plasmatocyte and crystal cell lineage differentiation (Fig S10D-H and J). Whereas treatment with mTOR inhibitor – Rapamycin for 16 hours led to a decrease in plasmatocyte and crystal cell differentiation, compared to the control treatment (Fig 7G-L). While genetically depleting Tor did not result in any significant change in plasmatocyte and crystal cell differentiation, Raptor depletion resulted in a decrease in crystal cell differentiation whereas no significant change was observed with respect to plasmatocyte differentiation (Fig S10A-B, E-F and I). Also, Tep4 progenitor specific knockdown of Tor and Raptor did not have any non-cell autonomous effect on niche numbers. On the other hand, mTOR activation via Rheb resulted in a non-cell autonomous decrease in niche numbers as compared to the wildtype (Fig S11A-D, I). Abrogation of mTOR signaling by tep4-Gal4 mediated depletion of Tor resulted in a decrease in γ-H2Ax positive puncta in the LG whereas Raptor depletion or Rheb over-expression did not have any effect as compared to the wild type control (Fig S11E-H, J).

Gcn5 acts as a nutrient sensor and is regulated by mTORC1

Enzymatic activity of Gcn5 is regulated by the cellular and metabolic energy state which in turn controls gene expression programs[65]. Gcn5 is capable of sensing Acetyl Co-A which is a central metabolic intermediate[75]. Since Gcn5 levels are critical in controlling gene expression programs and transcriptional noise[76], we tested if Gcn5 levels are responsive to altered nutrient conditions. We subjected *Drosophila* larvae to different dietary conditions viz. Fed, starved and high fat diet (HFD) and probed for Gcn5 levels in these conditions. Our results indicate that there is a decrease in Gcn5 levels upon starvation whereas an increase in high fat diet (HFD) conditions (Fig 7M, O) Gcn5 levels were normalized to β- actin in the fed, starved and high diet scenario (Fig 7O) and upon Rapamycin treatment (Fig 7P). mTOR is known to control protein translation in response to nutrient stress signals; under nutrient deprivation, mTOR is inhibited thereby inducing autophagy.

There are few studies that have linked mTOR to histone acetyltransferase Gcn5 and therefore nutrient response[59,77] . To further determine if Gcn5 levels are regulated by mTORC1 activity, we treated larvae with mTOR inhibitor Rapamycin and probed for Gcn5 levels. We found that there was a decrease in Gcn5 levels upon mTOR inhibition as compared to control (Fig 7N, P).

mTORC1 overrides the effect of Gcn5 in regulating blood cell homeostasis in the LG

mTORC1 regulates autophagy at multiple nodal points for example by phosphorylation of initiator kinase ULK1 or by phosphorylating TFEB preventing its nuclear translocation. On the other hand, Gcn5 regulates autophagy by acetylation of TFEB preventing its dimerization and nuclear translocation thereby inhibiting autophagy[59]. Since both mTORC1 and Gcn5 converge on and exert their effect over TFEB by phosphorylation or acetylation respectively, we wanted to investigate if one can override the effector function of the other. Since our results indicate that mTOR activity can regulate Gcn5 levels, we wanted to test if mTORC1 can override the effect of Gcn5 modulation in controlling LG hematopoiesis. Activation of mTOR by treatment with 3BDO in tep4-Gal4 mediated prohemocyte specific Gcn5 knockdown genetic background led to increased plasmatocyte and crystal cell differentiation as compared to the tep4-Gal4 mediated prohemocyte specific Gcn5 knockdown control (Fig 8A-D', I and J). Similarly, inhibition of mTOR by Rapamycin treatment in the dome-Gal4 mediated prohemocyte specific Gcn5 over-expression genetic background resulted in a significant reduction in plasmatocyte and crystal cell differentiation as compared to the dome-Gal4 mediated prohemocyte specific Gcn5 over-expression control (Fig 8E-H', K and L). This over-riding effect is based on chemical intervention data and would need further genetic experiments to fully establish the regulatory role of mTORC1. Taken together, our results demonstrate that a fine balance between mTORC1 mediated phosphorylation of TFEB and Gcn5 mediated acetylation of TFEB maintains the autophagic flux. Nutrient conditions, mTORC1 activity and Gcn5 levels are key determinants of autophagic flux in the LG. Maintenance of the autophagic flux and turnover is critical for regulating blood cell homeostasis in the LG. Thus, Gcn5-mTOR-TFEB signaling axis controls autophagy thereby regulating *Drosophila* blood cell homeostasis in the LG (Fig 9).

Discussion

Gcn5 is highly expressed in acute myeloid leukemia (AML) and helps in the maintenance of immature leukemic blasts [54,55]. While its function in the context of leukemia is well studied, Gcn5 function during physiological hematopoiesis is unexplored. Here, we explore Gcn5 role during normal physiological hematopoiesis in *Drosophila*. Our work shows that Gcn5, a histone acetyltransferase plays an important role during *Drosophila* LG hematopoiesis. We find that Gcn5 is expressed in all the LG cellular subsets and its levels are critical for controlling hematopoiesis. Structure-function analysis of Gcn5 shows that expression of Gcn5 lacking any of its constituent domains in wild type genetic background results in a dominant negative phenotype in the LG. Our results indicate that optimum levels of Gcn5 are critical in the prohemocytes as excess Gcn5 results in increased blood cell differentiation. We find that the number of PSC cells are altered either in an autonomous or non-autonomous manner where PSC-specific or non-PSC- specific modulation of Gcn5 levels results in changes in niche cell numbers which could be due to perturbation of signaling pathways like Insulin, mTOR, Dpp which are critical in maintaining the niche cells [21,78] which needs further exploration. Our results also suggest that niche cells numbers are reduced in the *gcn5* null mutants and transheterozygotes of *gcn5* mutant alleles which we speculate could be due to abrogation of signals like Insulin, mTOR or Dpp that are important for PSC maintenance. Since these are whole animal mutants there could be a number of signals that could be perturbed which needs to be investigated. Our results show that there is increased differentiation in *gcn5* mutant alleles and transheterozygotes which could be due to abrogation of various signaling pathways that might be affected systemically and LGs are highly sensitive to systemic signals which could result in aberrant hematopoiesis which needs further investigation. Also, we observe that PSC numbers are modulated upon perturbation of Gcn5 using *HmlΔ-Gal4* which could be a reciprocal mode of niche regulation however characterization of these signals would need further investigation. Further, we find that Gcn5 acts as a nutrient sensor and its levels are critical for controlling the autophagic flux in the LG. In order to investigate whether autophagy players regulate LG hematopoiesis, we carried out a systematic genetic perturbation analysis of key autophagy genes and our results indicate that disrupting autophagy abrogates LG hematopoiesis. Increased Gcn5 levels in the hemocytes led to a decrease in the autophagic flux whereas depleting Gcn5 resulted in increased autophagy which also correlates with the corresponding LG hematopoietic phenotypes.

Since mTORC1 regulates autophagy in response to nutrient conditions, we investigated whether modulating mTORC1 activity affects hematopoiesis. Our data elucidates that modulating mTORC1 activity regulates hematopoiesis and these effects are consistent with observations obtained upon genetic modulation of autophagy. Inhibiting mTORC1 activity using Rapamycin results in Gcn5 down-regulation establishing a regulatory link between mTORC1 and Gcn5. One of the common molecular link through which both mTORC1 and Gcn5 could potentially regulate autophagy is through Transcription factor EB (TFEB), a member of the microphthalmia-associated transcription factor/transcription factor E (MiTF/TFE) family[79] . Our results demonstrate that mTORC1 can override Gcn5 in regulating LG hematopoiesis. Although we show this over-ride effect with chemical intervention, further genetic epistasis-based analysis will further strengthen this data providing important insights.

Overall, we demonstrate that the Gcn5-TFEB-mTORC1 signaling axis regulates *Drosophila* LG hematopoiesis via its control over autophagy.

Expression analysis of Gcn5 in the LG indicates that Gcn5 is expressed in all the LG cellular sub-populations. *gcn5* mutant alleles display loss of blood cell homeostasis.. Increase in plasmatocyte or crystal cell differentiation could be due to a contribution of systemic signals that are altered upon loss of Gcn5 in the entire organism as the LG is capable of responding to external stimuli[80] . *gcn5* mutant alleles either in homozygous or trans-heterozygous conditions show an increased accumulation of DNA damage indicative of its role in DNA damage repair pathways[49,81]. Prohemocyte-specific over-expression of Gcn5 leads to increased plasmatocyte as well as crystal cell differentiation whereas depletion of Gcn5 levels has no significant effect on differentiation. *Hmldelta-Gal4* mediated Cortical Zone (CZ) specific over- expression of Gcn5 resulted in a cell autonomous increase in crystal cell differentiation whereas Gcn5 knockdown had no effect. These results show that optimum levels of Gcn5 are important for maintaining LG blood cell homeostasis. Higher levels of Gcn5 skews the balance towards increased blood cell differentiation. Higher Gcn5 expression has been observed previously in many carcinomas and leukemia promoting cell proliferation, growth and cancer progression [50–55]. Structure- function analysis shows that expression of Gcn5 lacking the Bromo or Ada domain in the wild type genetic background results in a dominant negative phenotype in terms of the maintenance of prohemocyte population itself and plasmatocyte differentiation whereas expression of Gcn5 lacking HAT or Bromo or Ada results in a dominant negative effect on crystal cell differentiation indicating that the constituent domains of Gcn5 might be playing specific functions in regulating various aspects of LG hematopoiesis via specific interacting partners. The constituent domains in Gcn5 could be performing unique functions in regulating homeostasis based on their interacting partners which needs to be explored. Gcn5 responds to changes in cellular energetic and metabolic states [65]. Gcn5 via its non-histone acetylation target, Transcription factor EB (TFEB) is capable of regulating autophagy which is directly linked to the nutritional status of the cell. Since Gcn5 is capable of sensing nutrient signals, its role in regulating the sensing by blood progenitors needs to be studied in detail and if it has any other potential crosstalk with signaling pathways that act downstream of nutrient and metabolic signals. TFEB acetylation by Gcn5 is inhibitory for TFEB as it prevents its dimerization and hence nuclear translocation. Upon nuclear translocation, TFEB activates genes responsible for autophagosome and lysosome biogenesis[59] .

In order to probe whether Gcn5 mediated regulation is due to its control over autophagy, we probed whether perturbing Gcn5 has any effect on the autophagic flux in the hemocytes. Our results suggest that depletion of Gcn5 leads to an upregulation of autophagy increasing the flux whereas over- expression of Gcn5 results in downregulation of autophagy lowering the autophagic flux. These observations were intriguing as this establishes an important role of autophagy in maintaining LG homeostasis. We investigated this further to find out if there is a direct link between autophagy regulators (Atg genes) including TFEB in controlling LG hematopoiesis. Genetic perturbation of the autophagy pathway regulators or TFEB in the prohemocytes leads to an increase in blood cell differentiation. Chemical inhibition of autophagy induced by Chloroquine also recapitulates this phenotype. There is literature indicating a critical role for autophagy in development of the blood system, self-renewal of HSCs and their mobilization[27,30,31,35] . Our observations on the role of autophagy in *Drosophila* LG hematopoiesis support these findings. We

then moved on to test if mTORC1 could regulate hematopoiesis. Chemical or genetic modulation of mTORC1 activity which is a master molecule that regulates autophagy alters LG hematopoiesis. mTORC1 activity regulates Gcn5 levels as inhibition of mTORC1 activity resulted in lower levels of Gcn5.

mTORC1 regulates autophagy via two arms - One via the initiator kinase, Ulk1 in response to either nutrient depletion or replete conditions via inhibitory phosphorylation of TFEB[71–73] . TFEB phosphorylation by mTORC1 subjects it to degradation thereby inhibiting autophagy[82]. Since TFEB is the common link that is regulated by both mTORC1 and Gcn5, we wanted to understand whether one is epistatic to the other in controlling hematopoiesis. We find that mTORC1 can override Gcn5 in controlling hematopoiesis by chemical intervention approach. Although, further genetic epistasis experiments will be needed to show that this effect is indeed by acting upstream and controlling Gcn5. We speculate that during physiological hematopoiesis a balance between phosphorylation and acetylation of TFEB mediated by mTORC1 and Gcn5 respectively regulates levels of autophagy. Perturbation of Gcn5 or mTORC1 activity could disturb this balance thereby deregulating hematopoiesis. Our findings shed light on the importance of non-histone acetylation function of Gcn5 in hematopoiesis. This could especially be important as the LG prohemocytes are known to respond to cell intrinsic and extrinsic nutrient signals[20]. The nutrient state could regulate autophagy thereby dictating the differentiation trajectory of the precursor cells. Since Gcn5 is highly expressed in acute myeloid leukemia[54,55] it becomes important to understand how Gcn5 level is regulated and what cellular processes Gcn5 is capable of regulating in order to control tissue homeostasis. Our work sheds novel insights on the role of Gcn5 during normal hematopoiesis. Our results illustrate that Gcn5 in the LG is capable of sensing and responding to external stimuli by calibrating the levels of autophagy in blood cells. It would be interesting to understand the kind of nutrient signals to which Gcn5 is capable of responding and whether Gcn5 has any crosstalk with other nutrient sensing molecules and pathways other than mTORC1. The nutrient sensing function of Gcn5 given the ability of hemocytes to respond to nutrient cues warrants further investigation. We show that Gcn5 fine tunes autophagy in conjunction with mTORC1 where mTORC1 activity is capable of regulating Gcn5 and can override its function in modulating autophagy. It would be interesting to further understand how an optimal balance of phosphorylation or acetylation of TFEB by mTORC1 or Gcn5 respectively modulates the resultant autophagic flux in order to control various cellular functions like stem cell homeostasis. Our findings shed light on the importance of non-histone acetylation function of Gcn5 in a vital process like hematopoiesis. Overall, our work uncovers a novel Gcn5-mTORC1-TFEB signaling axis that regulates *Drosophila* hematopoiesis via its control over autophagy (Figure 9).

Materials and Methods:

List of *Drosophila* stocks, antibodies used for immunofluorescence-based experiments have been listed in a detailed manner in the Supplemental Information (SI). The experimental protocol for lymph gland dissection, immunohistochemistry and image analysis has been mentioned in the SI. The procedure for protein extraction, western blotting and quantitative real time PCR has been mentioned in the SI along with the list of primers used for qRT experiments. The chemical treatment procedure has been described in a detailed manner in the SI. Statistical analysis performed for each of the experiments has been described in the statistical analysis section in the SI.

Data, Materials, and Software availability:

All the data related to this study are included in the article and/or in the SI.

Acknowledgements:

We thank the Bloomington Drosophila Stock Center, Developmental Studies Hybridoma Bank and the fly community for fly stocks and antibodies. We would particularly like to thank Clement Carre, Lucas Waltzer, Mohit Prasad and Bhupendra Shravage for help with fly stocks. We would like to thank the core central facilities and the technical support staff at ACTREC – Tata Memorial Centre. We also thank our lab members for critical discussions. This work was funded by Basic and Translational Research in Cancer grant (No.1/3(7)/2020/TMC/R&D-II/8823 Dt.30.07.2021), Capacity Building and Development of Novel and Cutting-edge Research Activities (No.1/3(4)/2021/TMC/R&D- II/15063 Dt.15.12.2021) from Department of Atomic Energy (DAE), Government of India.

Author contributions:

Conceptualization: AAR and RJK; Methodology: AAR, MK, SM and LK; Validation: AAR, MK; Formal analysis: AAR, MK, SM and LK; Investigation: AAR, MK, SM and LK; Resources: RJK ; Data curation: AAR, MK; Writing - original draft: AAR, MK RJK; Writing - review & editing: AAR, MK and RJK; Visualization: AAR and RJK; Supervision: RJK; Project administration: RJK; Funding acquisition: RJK

Competing interests:

The authors declare no competing or financial interests

References:

(1) Banerjee, U.; Girard, J. R.; Goins, L. M.; Spratford, C. M. *Drosophila* as a Genetic Model for Hematopoiesis. *Genetics* **2019**, *211* (2), 367–417. https://doi.org/10.1534/genetics.118.300223.

(2) Evans, C. J.; Hartenstein, V.; Banerjee, U. Thicker Than Blood. *Dev. Cell* **2003**, *5* (5), 673–690. https://doi.org/10.1016/S1534-5807(03)00335-6.

(3) Jung, S.-H.; Evans, C. J.; Uemura, C.; Banerjee, U. The *Drosophila* Lymph Gland as a Developmental Model of Hematopoiesis. *Development* **2005**, *132* (11), 2521–2533. https://doi.org/10.1242/dev.01837.

(4) Cho, B.; Yoon, S.-H.; Lee, D.; Koranteng, F.; Tattikota, S. G.; Cha, N.; Shin, M.; Do, H.; Hu, Y.; Oh, S. Y.; Lee, D.; Vipin Menon, A.; Moon, S. J.; Perrimon, N.; Nam, J.-W.; Shim, J. Single-Cell Transcriptome Maps of Myeloid Blood Cell Lineages in Drosophila. *Nat. Commun.* **2020**, *11* (1), 4483. https://doi.org/10.1038/s41467-020-18135-y.

(5) Kharrat, B.; Csordás, G.; Honti, V. Peeling Back the Layers of Lymph Gland Structure and Regulation. *Int. J. Mol. Sci.* **2022**, *23* (14), 7767. https://doi.org/10.3390/ijms23147767.

(6) Girard, J. R.; Goins, L. M.; Vuu, D. M.; Sharpley, M. S.; Spratford, C. M.; Mantri, S. R.; Banerjee, U. Paths and Pathways That Generate Cell-Type Heterogeneity and Developmental Progression in Hematopoiesis. *eLife* **2021**, *10*, e67516. https://doi.org/10.7554/eLife.67516.

(7) Dey, N. S.; Ramesh, P.; Chugh, M.; Mandal, S.; Mandal, L. Dpp Dependent Hematopoietic Stem Cells Give Rise to Hh Dependent Blood Progenitors in Larval Lymph Gland of Drosophila. *eLife* **2016**, *5*, e18295. https://doi.org/10.7554/eLife.18295.

(8) Khadilkar, R. J.; Rodrigues, D.; Mote, R. D.; Sinha, A. R.; Kulkarni, V.; Magadi, S. S.; Inamdar, M. S. ARF1–GTP Regulates Asrij to Provide Endocytic Control of *Drosophila* Blood Cell Homeostasis. *Proc. Natl. Acad. Sci.* **2014**, *111* (13), 4898–4903. https://doi.org/10.1073/pnas.1303559111.

(9) Khadilkar, R. J.; Vogl, W.; Goodwin, K.; Tanentzapf, G. Modulation of Occluding Junctions Alters the Hematopoietic Niche to Trigger Immune Activation. *eLife* **2017**, *6*, e28081. https://doi.org/10.7554/eLife.28081.

(10) Khadilkar, R. J.; Ho, K. Y. L.; Venkatesh, B.; Tanentzapf, G. Integrins Modulate Extracellular Matrix Organization to Control Cell Signaling during Hematopoiesis. *Curr. Biol.* **2020**, *30* (17), 3316-3329.e5. https://doi.org/10.1016/j.cub.2020.06.027.

(11) Khadilkar, R. J.; Tanentzapf, G. Septate Junction Components Control *Drosophila* Hematopoiesis through the Hippo Pathway. *Development* **2019**, *146* (7), dev166819. https://doi.org/10.1242/dev.166819.

(12) Krzemień, J.; Dubois, L.; Makki, R.; Meister, M.; Vincent, A.; Crozatier, M. Control of Blood Cell Homeostasis in Drosophila Larvae by the Posterior Signalling Centre. *Nature* **2007**, *446* (7133), 325–328. https://doi.org/10.1038/nature05650.

(13) Mandal, L.; Martinez-Agosto, J. A.; Evans, C. J.; Hartenstein, V.; Banerjee, U. A Hedgehog- and Antennapedia-Dependent Niche Maintains Drosophila Haematopoietic Precursors. *Nature* **2007**, *446* (7133), 320–324. https://doi.org/10.1038/nature05585.

(14) Sinenko, S. A.; Mandal, L.; Martinez-Agosto, J. A.; Banerjee, U. Dual Role of Wingless Signaling in Stem-like Hematopoietic Precursor Maintenance in Drosophila. *Dev. Cell* **2009**, *16* (5), 756–763. https://doi.org/10.1016/j.devcel.2009.03.003.

(15) Sinha, A.; Khadilkar, R. J.; S., V. K.; RoyChowdhury Sinha, A.; Inamdar, M. S. Conserved Regulation of the JAK/STAT Pathway by the Endosomal Protein Asrij Maintains Stem Cell Potency. *Cell Rep.* **2013**, *4* (4), 649–658. https://doi.org/10.1016/j.celrep.2013.07.029.

(16) Amcheslavsky, A.; Jiang, J.; Ip, Y. T. Tissue Damage-Induced Intestinal Stem Cell Division in Drosophila. *Cell Stem Cell* **2009**, *4* (1), 49–61. https://doi.org/10.1016/j.stem.2008.10.016.

(17) Chell, J. M.; Brand, A. H. Nutrition-Responsive Glia Control Exit of Neural Stem Cells from Quiescence. *Cell* **2010**, *143* (7), 1161–1173. https://doi.org/10.1016/j.cell.2010.12.007.

(18) McLeod, C. J.; Wang, L.; Wong, C.; Jones, D. L. Stem Cell Dynamics in Response to Nutrient Availability. *Curr. Biol.* **2010**, *20* (23), 2100–2105. https://doi.org/10.1016/j.cub.2010.10.038.

(19) Sousa-Nunes, R.; Yee, L. L.; Gould, A. P. Fat Cells Reactivate Quiescent Neuroblasts via TOR and Glial Insulin Relays in Drosophila. *Nature* **2011**, *471* (7339), 508–512. https://doi.org/10.1038/nature09867.

(20) Shim, J.; Mukherjee, T.; Banerjee, U. Direct Sensing of Systemic and Nutritional Signals by Haematopoietic Progenitors in Drosophila. *Nat. Cell Biol.* **2012**, *14* (4), 394–400.

https://doi.org/10.1038/ncb2453.
(21) Benmimoun, B.; Polesello, C.; Waltzer, L.; Haenlin, M. Dual Role for Insulin/TOR Signaling in the Control of Hematopoietic Progenitor Maintenance in *Drosophila*. *Development* **2012**, *139* (10), 1713–1717. https://doi.org/10.1242/dev.080259.
(22) Dragojlovic-Munther, M.; Martinez-Agosto, J. A. Multifaceted Roles of PTEN and TSC Orchestrate Growth and Differentiation of *Drosophila* Blood Progenitors. *Development* **2012**, *139* (20), 3752–3763. https://doi.org/10.1242/dev.074203.
(23) Tokusumi, Y.; Tokusumi, T.; Shoue, D. A.; Schulz, R. A. Gene Regulatory Networks Controlling Hematopoietic Progenitor Niche Cell Production and Differentiation in the Drosophila Lymph Gland. *PLoS ONE* **2012**, *7* (7), e41604. https://doi.org/10.1371/journal.pone.0041604.
(24) Das, G.; Shravage, B. V.; Baehrecke, E. H. Regulation and Function of Autophagy during Cell Survival and Cell Death. *Cold Spring Harb. Perspect. Biol.* **2012**, *4* (6), a008813–a008813. https://doi.org/10.1101/cshperspect.a008813.
(25) Lu, G.; Wang, Y.; Shi, Y.; Zhang, Z.; Huang, C.; He, W.; Wang, C.; Shen, H. Autophagy in Health and Disease: From Molecular Mechanisms to Therapeutic Target. *MedComm* **2022**, *3* (3), e150. https://doi.org/10.1002/mco2.150.
(26) Dossou, A. S.; Basu, A. The Emerging Roles of mTORC1 in Macromanaging Autophagy. *Cancers* **2019**, *11* (10), 1422. https://doi.org/10.3390/cancers11101422.
(27) Ho, T. T.; Warr, M. R.; Adelman, E. R.; Lansinger, O. M.; Flach, J.; Verovskaya, E. V.; Figueroa, M. E.; Passegué, E. Autophagy Maintains the Metabolism and Function of Young and Old Stem Cells. *Nature* **2017**, *543* (7644), 205–210. https://doi.org/10.1038/nature21388.
(28) Mortensen, M.; Soilleux, E. J.; Djordjevic, G.; Tripp, R.; Lutteropp, M.; Sadighi-Akha, E.; Stranks, A. J.; Glanville, J.; Knight, S.; W. Jacobsen, S.-E.; Kranc, K. R.; Simon, A. K. The Autophagy Protein Atg7 Is Essential for Hematopoietic Stem Cell Maintenance. *J. Exp. Med.* **2011**, *208* (3), 455–467. https://doi.org/10.1084/jem.20101145.
(29) Warr, M. R.; Binnewies, M.; Flach, J.; Reynaud, D.; Garg, T.; Malhotra, R.; Debnath, J.; Passegué, E. FOXO3A Directs a Protective Autophagy Program in Haematopoietic Stem Cells. *Nature* **2013**, *494* (7437), 323–327. https://doi.org/10.1038/nature11895.
(30) Gomez-Puerto, M. C.; Folkerts, H.; Wierenga, A. T. J.; Schepers, K.; Schuringa, J. J.; Coffer, P. J.; Vellenga, E. Autophagy Proteins ATG5 and ATG7 Are Essential for the Maintenance of Human CD34+ Hematopoietic Stem-Progenitor Cells. *Stem Cells* **2016**, *34* (6), 1651–1663. https://doi.org/10.1002/stem.2347.
(31) Liu, F.; Lee, J. Y.; Wei, H.; Tanabe, O.; Engel, J. D.; Morrison, S. J.; Guan, J.-L. FIP200 Is Required for the Cell-Autonomous Maintenance of Fetal Hematopoietic Stem Cells. *Blood* **2010**, *116* (23), 4806–4814. https://doi.org/10.1182/blood-2010-06-288589.
(32) Shravage, B. V.; Hill, J. H.; Powers, C. M.; Wu, L.; Baehrecke, E. H. *Atg6* Is Required for Multiple Vesicle Trafficking Pathways and Hematopoiesis in *Drosophila*. *Development* **2013**, *140* (6), 1321–1329. https://doi.org/10.1242/dev.089490.
(33) Kadandale, P.; Stender, J. D.; Glass, C. K.; Kiger, A. A. Conserved Role for Autophagy in Rho1-Mediated Cortical Remodeling and Blood Cell Recruitment. *Proc. Natl. Acad. Sci.* **2010**, *107* (23), 10502–10507. https://doi.org/10.1073/pnas.0914168107.
(34) Qin, B.; Yu, S.; Chen, Q.; Jin, L. H. Atg2 Regulates Cellular and Humoral Immunity in Drosophila. *Insects* **2023**, *14* (8), 706. https://doi.org/10.3390/insects14080706.
(35) Koschade, S. E.; Brandts, C. H. Selective Autophagy in Normal and Malignant Hematopoiesis. *J. Mol. Biol.* **2020**, *432* (1), 261–282. https://doi.org/10.1016/j.jmb.2019.06.025.
(36) Brownell, J. E.; Zhou, J.; Ranalli, T.; Kobayashi, R.; Edmondson, D. G.; Roth, S. Y.; Allis, C. D. Tetrahymena Histone Acetyltransferase A: A Homolog to Yeast Gcn5p Linking Histone Acetylation to Gene Activation. *Cell* **1996**, *84* (6), 843–851. https://doi.org/10.1016/S0092-8674(00)81063-6.
(37) Grant, P. A.; Eberharter, A.; John, S.; Cook, R. G.; Turner, B. M.; Workman, J. L. Expanded Lysine Acetylation Specificity of Gcn5 in Native Complexes. *J. Biol. Chem.* **1999**, *274* (9), 5895–5900. https://doi.org/10.1074/jbc.274.9.5895.
(38) Nagy, Z.; Tora, L. Distinct GCN5/PCAF-Containing Complexes Function as Co-Activators and Are Involved in Transcription Factor and Global Histone Acetylation. *Oncogene* **2007**, *26* (37), 5341–5357. https://doi.org/10.1038/sj.onc.1210604.
(39) Pearson, K. J.; Baur, J. A.; Lewis, K. N.; Peshkin, L.; Price, N. L.; Labinskyy, N.; Swindell, W. R.; Kamara, D.; Minor, R. K.; Perez, E.; Jamieson, H. A.; Zhang, Y.; Dunn, S. R.; Sharma, K.; Pleshko, N.;

Woollett, L. A.; Csiszar, A.; Ikeno, Y.; Le Couteur, D.; Elliott, P. J.; Becker, K. G.; Navas, P.; Ingram, D. K.; Wolf, N. S.; Ungvari, Z.; Sinclair, D. A.; De Cabo, R. Resveratrol Delays Age-Related Deterioration and Mimics Transcriptional Aspects of Dietary Restriction without Extending Life Span. *Cell Metab.* **2008**, *8* (2), 157–168. https://doi.org/10.1016/j.cmet.2008.06.011.

(40) Kuo, Y.-M.; Andrews, A. J. Quantitating the Specificity and Selectivity of Gcn5-Mediated Acetylation of Histone H3. *PLoS ONE* **2013**, *8* (2), e54896. https://doi.org/10.1371/journal.pone.0054896.

(41) Kollenstart, L.; De Groot, A. J. L.; Janssen, G. M. C.; Cheng, X.; Vreeken, K.; Martino, F.; Côté, J.; Van Veelen, P. A.; Van Attikum, H. Gcn5 and Esa1 Function as Histone Crotonyltransferases to Regulate Crotonylation-Dependent Transcription. *J. Biol. Chem.* **2019**, *294* (52), 20122–20134. https://doi.org/10.1074/jbc.RA119.010302.

(42) Wang, L.; Mizzen, C.; Ying, C.; Candau, R.; Barlev, N.; Brownell, J.; Allis, C. D.; Berger, S. L. Histone Acetyltransferase Activity Is Conserved between Yeast and Human GCN5 and Is Required for Complementation of Growth and Transcriptional Activation. *Mol. Cell. Biol.* **1997**, *17* (1), 519–527. https://doi.org/10.1128/MCB.17.1.519.

(43) Wang, Y.; Guo, Y. R.; Liu, K.; Yin, Z.; Liu, R.; Xia, Y.; Tan, L.; Yang, P.; Lee, J.-H.; Li, X.; Hawke, D.; Zheng, Y.; Qian, X.; Lyu, J.; He, J.; Xing, D.; Tao, Y. J.; Lu, Z. KAT2A Coupled with the α-KGDH Complex Acts as a Histone H3 Succinyltransferase. *Nature* **2017**, *552* (7684), 273–277. https://doi.org/10.1038/nature25003.

(44) Huang, B.; Zhong, D.; Zhu, J.; An, Y.; Gao, M.; Zhu, S.; Dang, W.; Wang, X.; Yang, B.; Xie, Z. Inhibition of Histone Acetyltransferase GCN5 Extends Lifespan in Both Yeast and Human Cell Lines. *Aging Cell* **2020**, *19* (4), e13129. https://doi.org/10.1111/acel.13129.

(45) Lerin, C.; Rodgers, J. T.; Kalume, D. E.; Kim, S.; Pandey, A.; Puigserver, P. GCN5 Acetyltransferase Complex Controls Glucose Metabolism through Transcriptional Repression of PGC-1α. *Cell Metab.* **2006**, *3* (6), 429–438. https://doi.org/10.1016/j.cmet.2006.04.013.

(46) Gao, B.; Kong, Q.; Zhang, Y.; Yun, C.; Dent, S. Y. R.; Song, J.; Zhang, D. D.; Wang, Y.; Li, X.; Fang, D. The Histone Acetyltransferase Gcn5 Positively Regulates T Cell Activation. *J. Immunol.* **2017**, *198* (10), 3927–3938. https://doi.org/10.4049/jimmunol.1600312.

(47) Downey, M.; Knight, B.; Vashisht, A. A.; Seller, C. A.; Wohlschlegel, J. A.; Shore, D.; Toczyski, D. P. Gcn5 and Sirtuins Regulate Acetylation of the Ribosomal Protein Transcription Factor Ifh1. *Curr. Biol.* **2013**, *23* (17), 1638–1648. https://doi.org/10.1016/j.cub.2013.06.050.

(48) Wu, Y.; Ma, S.; Xia, Y.; Lu, Y.; Xiao, S.; Cao, Y.; Zhuang, S.; Tan, X.; Fu, Q.; Xie, L.; Li, Z.; Yuan, Z. Loss of GCN5 Leads to Increased Neuronal Apoptosis by Upregulating E2F1- and Egr-1-Dependent BH3-Only Protein Bim. *Cell Death Dis.* **2017**, *8* (1), e2570–e2570. https://doi.org/10.1038/cddis.2016.465.

(49) Guo, R.; Chen, J.; Mitchell, D. L.; Johnson, D. G. GCN5 and E2F1 Stimulate Nucleotide Excision Repair by Promoting H3K9 Acetylation at Sites of Damage. *Nucleic Acids Res.* **2011**, *39* (4), 1390–1397. https://doi.org/10.1093/nar/gkq983.

(50) Liu, K.; Zhang, Q.; Lan, H.; Wang, L.; Mou, P.; Shao, W.; Liu, D.; Yang, W.; Lin, Z.; Lin, Q.; Ji, T. GCN5 Potentiates Glioma Proliferation and Invasion via STAT3 and AKT Signaling Pathways. *Int. J. Mol. Sci.* **2015**, *16* (9), 21897–21910. https://doi.org/10.3390/ijms160921897.

(51) Majaz, S.; Tong, Z.; Peng, K.; Wang, W.; Ren, W.; Li, M.; Liu, K.; Mo, P.; Li, W.; Yu, C. Histone Acetyl Transferase GCN5 Promotes Human Hepatocellular Carcinoma Progression by Enhancing AIB1 Expression. *Cell Biosci.* **2016**, *6* (1), 47. https://doi.org/10.1186/s13578-016-0114-6.

(52) Mustachio, L. M.; Roszik, J.; Farria, A. T.; Guerra, K.; Dent, S. Y. Repression of GCN5 Expression or Activity Attenuates C-MYC Expression in Non-Small Cell Lung Cancer. *Am. J. Cancer Res.* **2019**, *9* (8), 1830–1845.

(53) Tzelepis, K.; Koike-Yusa, H.; De Braekeleer, E.; Li, Y.; Metzakopian, E.; Dovey, O. M.; Mupo, A.; Grinkevich, V.; Li, M.; Mazan, M.; Gozdecka, M.; Ohnishi, S.; Cooper, J.; Patel, M.; McKerrell, T.; Chen, B.; Domingues, A. F.; Gallipoli, P.; Teichmann, S.; Ponstingl, H.; McDermott, U.; Saez-Rodriguez, J.; Huntly, B. J. P.; Iorio, F.; Pina, C.; Vassiliou, G. S.; Yusa, K. A CRISPR Dropout Screen Identifies Genetic Vulnerabilities and Therapeutic Targets in Acute Myeloid Leukemia. *Cell Rep.* **2016**, *17* (4), 1193–1205. https://doi.org/10.1016/j.celrep.2016.09.079.

(54) Kahl, M.; Brioli, A.; Bens, M.; Perner, F.; Kresinsky, A.; Schnetzke, U.; Hinze, A.; Sbirkov, Y.; Stengel, S.; Simonetti, G.; Martinelli, G.; Petrie, K.; Zelent, A.; Böhmer, F.-D.; Groth, M.; Ernst, T.; Heidel, F. H.; Scholl, S.; Hochhaus, A.; Schenk, T. The Acetyltransferase GCN5 Maintains ATRA-Resistance in Non-APL AML. *Leukemia* **2019**, *33* (11), 2628–2639. https://doi.org/10.1038/s41375-

019-0581-y.
(55) Salunkhe, S.; Mishra, S. V.; Nair, J.; Ghosh, S.; Choudhary, N.; Kaur, E.; Shah, S.; Patkar, K.; Anand, D.; Khattry, N.; Hasan, S. K.; Dutt, S. Inhibition of Novel GCN5–ATM Axis Restricts the Onset of Acquired Drug Resistance in Leukemia. *Int. J. Cancer* **2018**, *142* (10), 2175–2185. https://doi.org/10.1002/ijc.31242.
(56) Smith, E. R.; Belote, J. M.; Schiltz, R. L.; Yang, X.-J.; Moore, P. A.; Berger, S. L.; Nakatani, Y.; Allis, C. D. Cloning of Drosophila GCN5: Conserved Features among Metazoan GCN5 Family Members. *Nucleic Acids Res.* **1998**, *26* (12), 2948–2954. https://doi.org/10.1093/nar/26.12.2948.
(57) Carré, C.; Szymczak, D.; Pidoux, J.; Antoniewski, C. The Histone H3 Acetylase dGcn5 Is a Key Player in *Drosophila Melanogaster* Metamorphosis. *Mol. Cell. Biol.* **2005**, *25* (18), 8228–8238. https://doi.org/10.1128/MCB.25.18.8228-8238.2005.
(58) Liu, T.; Wang, Q.; Li, W.; Mao, F.; Yue, S.; Liu, S.; Liu, X.; Xiao, S.; Xia, L. Gcn5 Determines the Fate of *Drosophila* Germline Stem Cells through Degradation of Cyclin A. *FASEB J.* **2017**, *31* (5), 2185–2194. https://doi.org/10.1096/fj.201601217R.
(59) Wang, Y.; Huang, Y.; Liu, J.; Zhang, J.; Xu, M.; You, Z.; Peng, C.; Gong, Z.; Liu, W. Acetyltransferase GCN5 Regulates Autophagy and Lysosome Biogenesis by Targeting TFEB. *EMBO Rep.* **2020**, *21* (1), e48335. https://doi.org/10.15252/embr.201948335.
(60) Rabanal-Ruiz, Y.; Otten, E. G.; Korolchuk, V. I. mTORC1 as the Main Gateway to Autophagy. *Essays Biochem.* **2017**, *61* (6), 565–584. https://doi.org/10.1042/EBC20170027.
(61) Woo, A. J.; Kim, J.; Xu, J.; Huang, H.; Cantor, A. B. Role of ZBP-89 in Human Globin Gene Regulation and Erythroid Differentiation. *Blood* **2011**, *118* (13), 3684–3693. https://doi.org/10.1182/blood-2011-03-341446.
(62) Tiwari, S. K.; Toshniwal, A. G.; Mandal, S.; Mandal, L. Fatty Acid β-Oxidation Is Required for the Differentiation of Larval Hematopoietic Progenitors in Drosophila. *eLife* **2020**, *9*, e53247. https://doi.org/10.7554/eLife.53247.
(63) Han, Y.; Zhao, H.; Li, G.; Jia, J.; Guo, H.; Tan, J.; Sun, X.; Li, S.; Ran, Q.; Bai, C.; Gu, Y.; Li, Z.; Guan, H.; Gao, S.; Zhou, P.-K. GCN5 Mediates DNA-PKcs Crotonylation for DNA Double-Strand Break Repair and Determining Cancer Radiosensitivity. *Br. J. Cancer* **2024**, *130* (10), 1621–1634. https://doi.org/10.1038/s41416-024-02636-4.
(64) Kendek, A.; Sandron, A.; Lambooij, J.-P.; Colmenares, S. U.; Pociunaite, S. M.; Gooijers, I.; de Groot, L.; Karpen, G. H.; Janssen, A. DNA Double-Strand Break Movement in Heterochromatin Depends on the Histone Acetyltransferase dGcn5. *Nucleic Acids Res.* **2024**, *52* (19), 11753–11767. https://doi.org/10.1093/nar/gkae775.
(65) Mutlu, B.; Puigserver, P. GCN5 Acetyltransferase in Cellular Energetic and Metabolic Processes. *Biochim. Biophys. Acta BBA - Gene Regul. Mech.* **2021**, *1864* (2), 194626. https://doi.org/10.1016/j.bbagrm.2020.194626.
(66) Galluzzi, L.; Yamazaki, T.; Kroemer, G. Linking Cellular Stress Responses to Systemic Homeostasis. *Nat. Rev. Mol. Cell Biol.* **2018**, *19* (11), 731–745. https://doi.org/10.1038/s41580-018-0068-0.
(67) Riffelmacher, T.; Simon, A. Mechanistic Roles of Autophagy in Hematopoietic Differentiation. *FEBS J.* **2017**, *284* (7), 1008–1020. https://doi.org/10.1111/febs.13962.
(68) Kang, Y.-A.; Sanalkumar, R.; O'Geen, H.; Linnemann, A. K.; Chang, C.-J.; Bouhassira, E. E.; Farnham, P. J.; Keles, S.; Bresnick, E. H. Autophagy Driven by a Master Regulator of Hematopoiesis. *Mol. Cell. Biol.* **2012**, *32* (1), 226–239. https://doi.org/10.1128/MCB.06166-11.
(69) Chen, C.; Liu, Y.; Liu, R.; Ikenoue, T.; Guan, K.-L.; Liu, Y.; Zheng, P. TSC–mTOR Maintains Quiescence and Function of Hematopoietic Stem Cells by Repressing Mitochondrial Biogenesis and Reactive Oxygen Species. *J. Exp. Med.* **2008**, *205* (10), 2397–2408. https://doi.org/10.1084/jem.20081297.
(70) Ianniciello, A.; Helgason, G. V. Targeting ULK1 in Cancer Stem Cells: Insight from Chronic Myeloid Leukemia. *Autophagy* **2022**, *18* (7), 1734–1736. https://doi.org/10.1080/15548627.2022.2041152.
(71) Ganley, I. G.; Lam, D. H.; Wang, J.; Ding, X.; Chen, S.; Jiang, X. ULK1·ATG13·FIP200 Complex Mediates mTOR Signaling and Is Essential for Autophagy. *J. Biol. Chem.* **2009**, *284* (18), 12297–12305. https://doi.org/10.1074/jbc.M900573200.
(72) Jung, C. H.; Jun, C. B.; Ro, S.-H.; Kim, Y.-M.; Otto, N. M.; Cao, J.; Kundu, M.; Kim, D.-H. ULK-Atg13-FIP200 Complexes Mediate mTOR Signaling to the Autophagy Machinery. *Mol. Biol. Cell* **2009**, *20* (7), 1992–2003. https://doi.org/10.1091/mbc.e08-12-1249.
(73) Kim, J.; Kundu, M.; Viollet, B.; Guan, K.-L. AMPK and mTOR Regulate Autophagy through Direct

Phosphorylation of Ulk1. *Nat. Cell Biol.* **2011**, *13* (2), 132–141. https://doi.org/10.1038/ncb2152.
(74) Napolitano, G.; Esposito, A.; Choi, H.; Matarese, M.; Benedetti, V.; Di Malta, C.; Monfregola, J.; Medina, D. L.; Lippincott-Schwartz, J.; Ballabio, A. mTOR-Dependent Phosphorylation Controls TFEB Nuclear Export. *Nat. Commun.* **2018**, *9* (1), 3312. https://doi.org/10.1038/s41467-018-05862-6.
(75) Schuetz, A.; Bernstein, G.; Dong, A.; Antoshenko, T.; Wu, H.; Loppnau, P.; Bochkarev, A.; Plotnikov, A. N. Crystal Structure of a Binary Complex between Human GCN5 Histone Acetyltransferase Domain and Acetyl Coenzyme A. *Proteins Struct. Funct. Bioinforma.* **2007**, *68* (1), 403–407. https://doi.org/10.1002/prot.21407.
(76) Raser, J. M.; O'Shea, E. K. Control of Stochasticity in Eukaryotic Gene Expression. *Science* **2004**, *304* (5678), 1811–1814. https://doi.org/10.1126/science.1098641.
(77) Laboucarié, T.; Detilleux, D.; Rodriguez-Mias, R. A.; Faux, C.; Romeo, Y.; Franz-Wachtel, M.; Krug, K.; Maček, B.; Villén, J.; Petersen, J.; Helmlinger, D. TORC1 and TORC2 Converge to Regulate the SAGA Co-activator in Response to Nutrient Availability. *EMBO Rep.* **2017**, *18* (12), 2197–2218. https://doi.org/10.15252/embr.201744942.
(78) Pennetier, D.; Oyallon, J.; Morin-Poulard, I.; Dejean, S.; Vincent, A.; Crozatier, M. Size Control of the *Drosophila* Hematopoietic Niche by Bone Morphogenetic Protein Signaling Reveals Parallels with Mammals. *Proc. Natl. Acad. Sci.* **2012**, *109* (9), 3389–3394. https://doi.org/10.1073/pnas.1109407109.
(79) Song, T.-T.; Cai, R.-S.; Hu, R.; Xu, Y.-S.; Qi, B.-N.; Xiong, Y.-A. The Important Role of TFEB in Autophagy-Lysosomal Pathway and Autophagy-Related Diseases: A Systematic Review. *Eur. Rev. Med. Pharmacol. Sci.* **2021**, *25* (3), 1641–1649. https://doi.org/10.26355/eurrev_202102_24875.
(80) Shim, J.; Gururaja-Rao, S.; Banerjee, U. Nutritional Regulation of Stem and Progenitor Cells in *Drosophila*. *Development* **2013**, *140* (23), 4647–4656. https://doi.org/10.1242/dev.079087.
(81) Zhao, M.; Geng, R.; Guo, X.; Yuan, R.; Zhou, X.; Zhong, Y.; Huo, Y.; Zhou, M.; Shen, Q.; Li, Y.; Zhu, W.; Wang, J. PCAF/GCN5-Mediated Acetylation of RPA1 Promotes Nucleotide Excision Repair. *Cell Rep.* **2017**, *20* (9), 1997–2009. https://doi.org/10.1016/j.celrep.2017.08.015.
(82) Martina, J. A.; Chen, Y.; Gucek, M.; Puertollano, R. MTORC1 Functions as a Transcriptional Regulator of Autophagy by Preventing Nuclear Transport of TFEB. *Autophagy* **2012**, *8* (6), 903–914. https://doi.org/10.4161/auto.19653.
1.

Main figure legends:

Figure 1. Gcn5 is expressed in all compartments of the *Drosophila* larval LG

Cartoon of the third instar larval LG, indicating the anterior primary lobes and the posterior lobes (A). The primary lobe of the LG depicting different subpopulations: the Posterior Signaling Centre (PSC: blue) functioning as the niche, Medullary zone (MZ: green) houses the progenitors, Intermediate progenitor zone (IZ: yellow) which contains the cells transitioning from progenitors to specific lineages, and the Cortical zone (CZ: brown) containing the differentiated hemocytes population – plasmatocytes and crystal cells (B). Gcn5 expression in different compartments of lymph gland (C-F'). Gcn5 (red) expression in the - Posterior Signaling Centre (PSC) using Collier-GFP (green) (C-C', E-E'), Medullary zone prohemocytes using Dome-GFP (green) (D-D', F-F'). Nuclei are stained with DAPI (Blue). Scale Bar: 50µm (C-D'), 30µm (E-F').

Figure 2. Whole animal *gcn5* mutants show defective LG homeostasis.

Posterior Signaling Center (PSC) cell numbers marked by Antennapedia (red) in *gcn5[C137Y/C137Y]* (B-B'), *gcn5[E333st/E333st]* (C-C') and *gcn5[E333st/C137Y]* (D-D'') as compared to wildtype (A-A'). Graphical representation of PSC cell numbers of the *gcn5* mutants as compared to the wildtype (E), n=24 for wildtype, n=37 for *gcn5[C137Y/C137Y]*, n=29 for *gcn5[E333st/E333st]* and n=20 for *gcn5[E333st/C137Y]* for PSC cell number quantification. Plasmatocyte differentiation was marked by P1 (red) in *gcn5[C137Y/C137Y]* (G-G'), *gcn5[E333st/E333st]* (H-H') and *gcn5[E333st/C137Y]* (I-I') as compared to the wildtype (F-F'). Graphical representation of plasmatocyte differentiation index of the *gcn5* mutants compared to wildtype (J), n=20 for wildtype, n=29 for *gcn5[C137Y/C137Y]*, n=33 for *gcn5[E333st/E333st]* and n=26 for *gcn5[E333st/C137Y]* for quantification. Crystal cell differentiation marked by Hnt (red) in *gcn5[C137Y/C137Y]* (L-L'), *gcn5[E333st/E333st]* (M-M') and *gcn5[E333st/C137Y]* (N-N') as compared to wildtype (K-K'). Graphical representation of crystal cell differentiation index for *gcn5* mutants compared to wildtype (O), n=22 for wildtype, n=26 for *gcn5[C137Y/C137Y]*, n=33 for *gcn5[E333st/E333st]* and n=31 for *gcn5[E333st/C137Y]* for quantification. Cells undergoing DNA damage marked by γH2AX (red) in *gcn5[C137Y/C137Y]* (Q-Q'), *gcn5[E333st/E333st]* (R-R') and *gcn5[E333st/C137Y]* (S-S') as compared to wildtype (P-P'). Graphical representation of γH2AX positive cells undergoing DNA damage in the gcn5 mutants compared to the wildtype (T), n=24 for wildtype, n=54 for *gcn5[C137YC137Y]*, n=41 for *gcn5[E333st/E333st]*and n=31 for *gcn5[E333st/C137Y]* for quantification. Nuclei are stained with DAPI (Blue). n represents the number of individual primary lobes of the LG. Individual data points in the graphs represent individual primary lobes of the LG. Values are mean ± SD, and asterisk marks statistically significant differences (*$p<0.05$; **$p<0.01$; ***$p<0.001$, ****$p<0.0001$, Student's t-test with Welch's correction). Scale Bar: 50µm (A-S'). Nuclei are stained with DAPI (blue). Scale Bar: 50µm (A-S').

Figure 3. Modulation of Gcn5 levels in the prohemocytes alters blood cell homeostasis in the lymph gland

Posterior Signalling Center (PSC) population marked by Antennapedia (red) upon Dome-Gal4 mediated knockdown (B-B') or over-expression (C-C') of Gcn5 as compared to wildtype (A- A'). Plasmatocyte differentiation marked by P1 (red) upon Dome-Gal4 mediated knockdown (E-E') or over-expression (F-F') of Gcn5 as compared to wildtype (D-D'). Crystal cell differentiation marked by Hnt (red) upon Dome-Gal4 mediated knockdown (H-H') or over- expression (I-I') of Gcn5 as compared to wild type (G-G'). Cells undergoing DNA damage marked by γH2AX (red) upon Dome-Gal4 mediated knockdown (K-K') or over-expression (L- L') of Gcn5 as compared

to wild type (J-J'). Graphical representation of PSC numbers upon modulation of Gcn5 levels in the Dome positive population compared to wildtype (M), n=28 for wildtype, n=28 for Gcn5 knockdown, and n=20 for Gcn5 over-expression. Graphical representation of prohemocyte index upon modulation of Gcn5 levels in dome population compared to wildtype (N), n=30 for wildtype, n=30 for Gcn5 knockdown, and n=30 for Gcn5 over-expression. Graphical representation of plasmatocyte differentiation index upon modulation of Gcn5 levels in dome population compared to wildtype (O), n=35 for wildtype, n=23 for Gcn5 knockdown, and n=25 for Gcn5 over-expression. Graphical representation of Crystal cell differentiation index upon modulation of Gcn5 levels in the dome population compared to wildtype (P), n=37 for wildtype, n=21 for Gcn5 knockdown, and n=33 for Gcn5 over-expression. Graphical representation of γH2AX positive cells upon modulation of Gcn5 levels in the dome population compared to wildtype (Q), n=33 for wildtype, n=27 for Gcn5 knockdown, and n=38 for Gcn5 over-expression. Nuclei are stained with DAPI (blue). Dome>GFP positive population (Green) indicates the expression domain of Dome-Gal4 activity in the LG. n represent the number of individual primary lobes of the LG. Individual data points in the graphs represent individual primary lobes of the Lymph Gland. Values are mean ± SD, and asterisk marks statistically significant differences (**p<0.01; ***p<0.001; ****p<0.0001, Student's t-test with Welch's correction). Scale Bar: 50µm (A-L').

Figure 4. Prohemocyte-specific expression of Gcn5 domain deletion constructs affects LG homeostasis.

Schematic of the SAGA HAT complex containing different modules – Sgf29, Ada2, Gcn5, and Ada3. Gcn5 is an 813 aa protein in Drosophila containing the Pcaf homology domain, HAT domain, Ada domain, and Bromodomain (A). Posterior Signalling Center (PSC) numbers marked by Antennapedia (red) upon expression of different Gcn5 domain deletion constructs in the tep-GFP (green) population using tep4-Gal4 (C-F), compared to wildtype (B). Progenitor index marked by tep (green) upon expression of different Gcn5 domain deletion constructs (C'- F'), compared to wildtype (B'). Plasmatocyte differentiation marked by P1 (red) upon expression of different Gcn5 domain deletion constructs in the tep-GFP population using tep4- Gal4 (green) (C"-F"), compared to wildtype (B"). Crystal cell differentiation marked by Hnt (red) upon expression of different Gcn5 domain deleted constructs in the tep-GFP population using tep4-Gal4 (green) (C"'-F"'), compared to wildtype (B"'). Graphical representation of PSC numbers upon expression of Gcn5 domain deletion constructs, compared to wildtype (G), n=40 for wildtype, n=29 for Gcn5ΔHAT expression, n=35 for Gcn5ΔPcaf expression, n=33 for Gcn5ΔBromo expression, and n=26 for Gcn5ΔAda expression in the tep population. Graphical representation of Prohemocyte index upon expression of Gcn5 domain deletion constructs, compared to wildtype (H), n=24 for wildtype, n=24 for Gcn5ΔHAT expression, n=34 for Gcn5ΔPcaf expression, n=24 for Gcn5ΔBromo expression, and n=24 for Gcn5ΔAda expression in the tep population. Graphical representation of Plasmatocyte differentiation index upon expression of Gcn5 domain deleted constructs, compared to wildtype (I), n=38 for wildtype, n=30 for Gcn5ΔHAT expression, n=29 for Gcn5ΔPcaf expression, n=27 for Gcn5ΔBromo expression, and n=27 for Gcn5ΔAda expression in the tep population. Graphical representation of Crystal cell numbers upon expression of Gcn5 domain deleted constructs, compared to wildtype (J), n=23 for wildtype, n=35 for Gcn5ΔHAT expression, n=26 for Gcn5ΔPcaf expression, n=26 for Gcn5ΔBromo expression, and n=26 for Gcn5ΔAda expression in the tep population. Nuclei are stained with DAPI (blue). n represent the number of individual primary lobes of the LG. Individual data points in the graphs represent individual primary lobes of the LG. Values are mean ± SD, and asterisk marks statistically significant differences (*p<0.05; **p<0.01; ***p<0.001; ****p<0.0001, Student's t-test with Welch's correction). Scale Bar: 50µm (B-F''').

Figure 5. Autophagic flux in *Drosophila* blood cells is negatively regulated by Gcn5

p62 (red) labeling the autophagy adaptor protein upon Hml-Gal4 mediated Gcn5 knockdown (B), or overexpression (C) as compared to wildtype (A). Atg8 (red), the autophagosomal marker upon Hml-Gal4 mediated Gcn5 knockdown (B') or over-expression (C') as compared to wildtype (A'). Nuclei were stained with DAPI (blue). Graphical representation of the p62 positive puncta/cell (D). Graphical representation of Atg8 positive puncta/cell (E). Values are mean ± SD, and asterisk marks statistically significant differences (***p<0.001; ****p<0.0001, Student's t-test with Welch's correction). Scale Bar: 20µm (A-E').

Figure 6. Genetic and chemical ablation of autophagy leads to aberrant blood cell differentiation.

Plasmatocyte differentiation marked by P1 (red) upon tep4-Gal4 mediated knockdown of TFEB (C-C'), Atg8a (E-E'), Atg5 (G-G'), or Atg18 (I-I') in the tep population (green) as compared to wildtype (A-A'). Crystal cell differentiation marked by Hnt (red) upon tep4-Gal4 mediated knockdown of TFEB (D-D'), Atg8a (F-F'), Atg5 (H-H'), or Atg18 (J-J') in the tep population (green) as compared to wildtype (B-B'). Graphical representation of Plasmatocyte differentiation index upon knockdown of TFEB (n=33), Atg8a (n=28), Atg5 (n=24), or Atg18 (n=22) in the tep population, compared to the wildtype (n=22) (K). Graphical representation of Crystal cell numbers upon knockdown of TFEB (n=21), Atg8a (n=44), Atg5 (n=30), or Atg18 (n=58) in the tep population, compared to the wildtype (n=28) (L). Plasmatocyte differentiation (red) upon Chloroquine treatment (N) as compared to control (M). Crystal cell differentiation upon Chloroquine treatment (P) as compared to control (O). Graphical representation of Plasmatocyte Differentiation Index upon Chloroquine treatment (n=30), compared to control (n=25) (Q). Graphical representation of Crystal Cell numbers upon Chloroquine treatment (n=25), compared to control (n=31) (R). Nuclei are stained with DAPI (blue). n represents the number of individual primary lobes of the LG. Individual data points in the graphs represent individual primary lobes of the LG. Values are mean ± SD, and asterisk marks statistically significant differences (*p<0.05; ***p<0.001; ****p<0.0001, Student's t- test with Welch's correction). Scale Bar: 50µm (A-P).

Figure 7. Modulation of mTORC1 activity regulates blood cell differentiation in the Lymph gland.

Plasmatocyte differentiation marked by P1 (red) upon 3BDO treatment (B-B') as compared to control (A-A'). Crystal cell differentiation marked by Hnt (red) upon 3BDO treatment (D-D') compared to control (C-C'). Graphical representation of Plasmatocyte Differentiation Index upon 3BDO treatment (n=28) compared to control (n=24) (E). Graphical representation of Crystal cell numbers upon 3BDO treatment (n=27) compared to control (n=24) (F). Plasmatocyte differentiation marked by P1 (red) upon Rapamycin treatment (H-H') compared to control (G-G'). Crystal cell differentiation marked by Hnt (red) upon Rapamycin treatment (J-J') compared to control (I-I'). Graphical representation of Plasmatocyte Differentiation Index upon Rapamycin treatment (n=28) compared to control (n=20) (K). Graphical representation of Crystal cell numbers upon Rapamycin treatment (n=25) compared to control (n=20) (L). Immunoblot showing GCN5 (93 kDa) protein levels in different diet conditions – fed, starved, and high-fat diet (M). Immunoblot showing GCN5 (93 kDa) protein levels upon Rapamycin treatment compared to wildtype (N). β-actin (42kDa) was used as the loading control. Nuclei are stained with DAPI (blue). Quantification of GCN5 protein levels in the fed, starved and High Fat diet scenario (O). Quantification of GCN5 protein levels in the wildtype as compared to rapamycin treatment (P). n

represent the number of individual primary lobes of the LG. Individual data points in the graphs represent individual primary lobes of the LG. Values are mean ± SD, and asterisk marks statistically significant differences (*p<0.05; **p<0.01; ***p<0.001; ****p<0.0001, Student's t-test with Welch's correction). Scale Bar: 50µm (A-J').

Figure 8. mTORC1 can override the effect of Gcn5 level modulation over autophagy.

Plasmatocyte differentiation marked by P1 (red) upon 3BDO treatment in tep4-Gal4 mediated (green) Gcn5 knockdown background (B-B') compared to control treatment in the same genetic background (A-A'). Crystal cell differentiation marked by Hnt (red) upon 3BDO treatment in the tep-mediated (green) Gcn5 knockdown background (D-D') compared to control treatment in the same genetic background (C-C'). Plasmatocyte differentiation marked by P1 (red) upon Rapamycin treatment in Dome-mediated (green) Gcn5 over-expression background (F-F') compared to control treatment in the same genetic background (E-E'). Crystal cell differentiation marked by Hnt (red) upon Rapamycin treatment in Dome-Gal4 mediated (green) Gcn5 over-expression background (H-H') as compared to control treatment in the same genetic background (G-G'). Graphical representation of Plasmatocyte Differentiation Index upon 3BDO treatment (n=21) and control treatment (n=20) in the tep- mediated Gcn5 knockdown background (I). Graphical representation of Crystal cell numbers upon 3BDO treatment (n=20) and control treatment (n=24) in the tep-mediated Gcn5 knockdown background (J). Graphical representation of Plasmatocyte Differentiation Index upon Rapamycin treatment (n=27) and control treatment (n=21) in the Dome-mediated Gcn5 over-expression background (K). Graphical representation of Crystal Cell numbers upon Rapamycin treatment (n=42) and control treatment (n=24) in the Dome-mediated Gcn5 over- expression background (L). Nuclei are stained with DAPI (blue). n represent the number of individual primary lobes of the LG. Individual data points in the graphs represent individual primary lobes of the LG. Values are mean ± SD, and asterisk marks statistically significant differences (**p<0.01; ***p<0.001, Student's t-test with Welch's correction). Scale Bar: 50µm (A-H').

Figure 9: Gcn5-mTORC1-TFEB signaling axis regulates autophagy to control blood cell homeostasis.

A cartoon summarizing how Gcn5-mTORC1-TFEB signaling axis regulates autophagy to control blood cell homeostasis in the Drosophila LG.

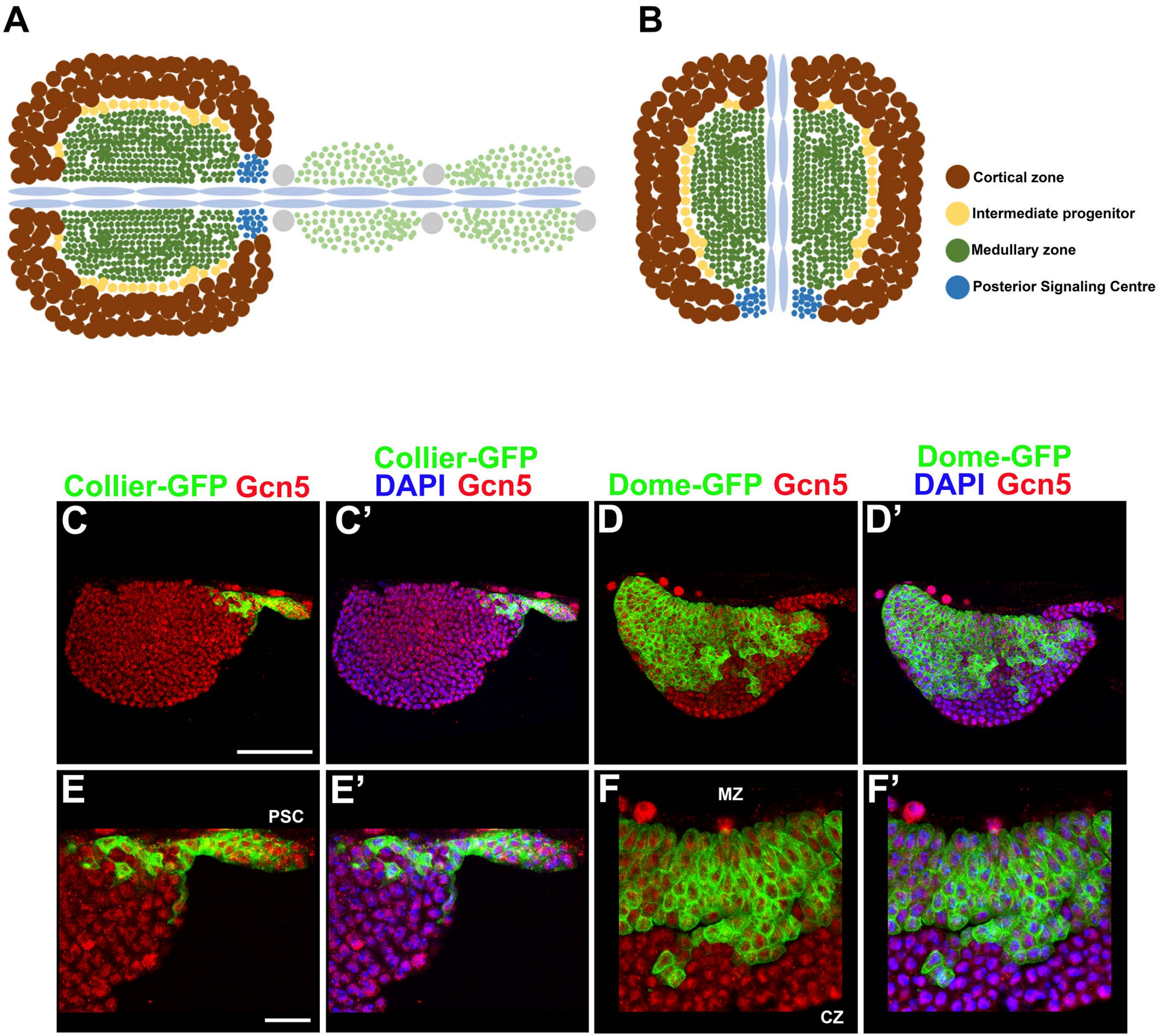
A
B
Cortical zone
Intermediate progenitor
Medullary zone
Posterior Signaling Centre
Collier-GFP Gcn5
Collier-GFP DAPI Gcn5
Dome-GFP Gcn5
Dome-GFP DAPI Gcn5
C
C'
D
D'
E
PSC
E'
F
MZ
CZ
F'

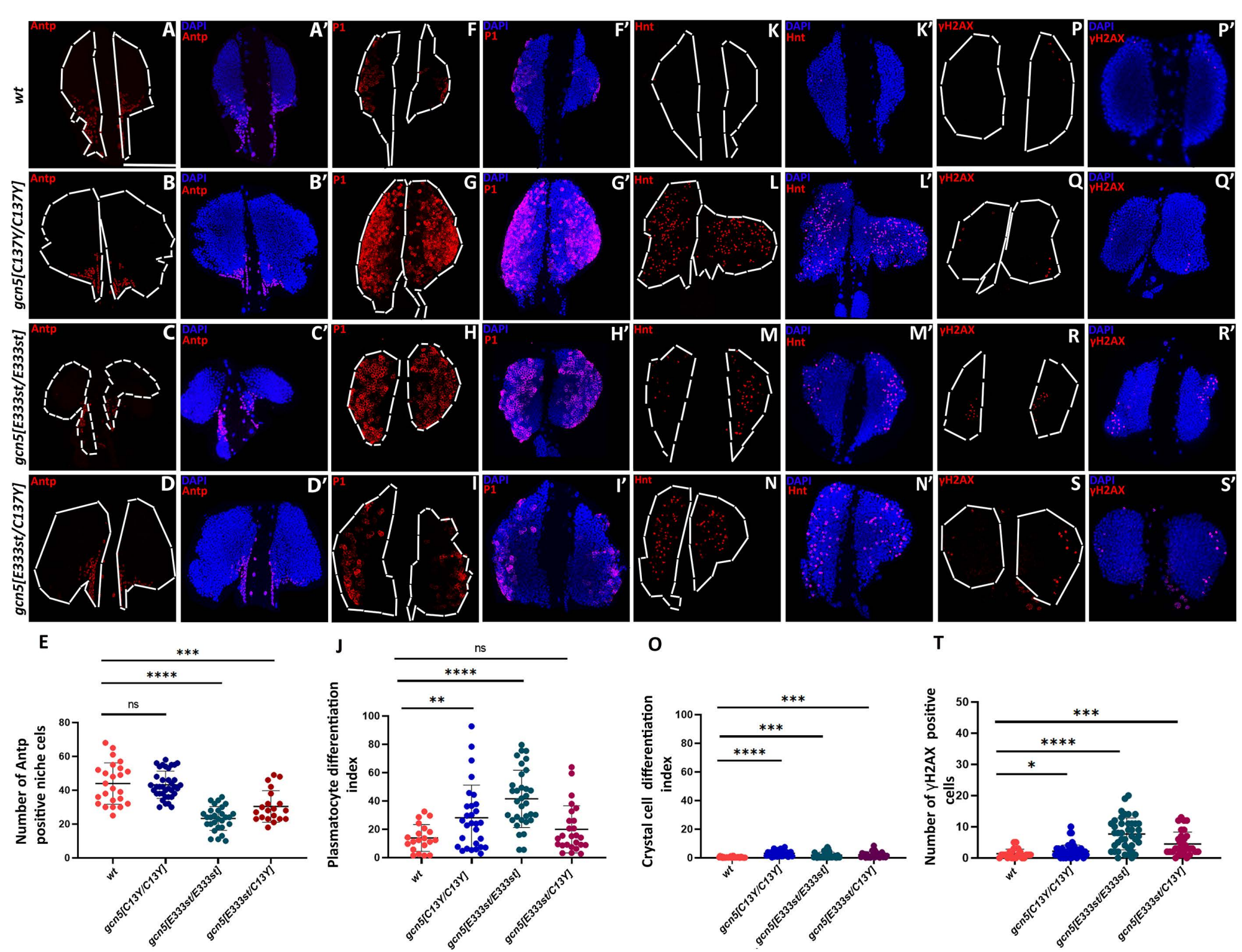
wt
gcn5[C137Y/C137Y]
gcn5[E333st/E333st]
gcn5[E333st/C137Y]
Antp
DAPI
P1
Hnt
γH2AX
A
A'
B
B'
C
C'
D
D'
F
F'
G
G'
H
H'
I
I'
K
K'
L
L'
M
M'
N
N'
P
P'
Q
Q'
R
R'
S
S'
E
Number of Antp positive niche cels
ns
****
***
J
Plasmatocyte differentiation index
**
****
ns
O
Crystal cell differentiation index
****
***
***
T
Number of γH2AX positive cells
*
****
***
wt
gcn5[C13Y/C13Y]
gcn5[E333st/E333st]
gcn5[E333st/C13Y]

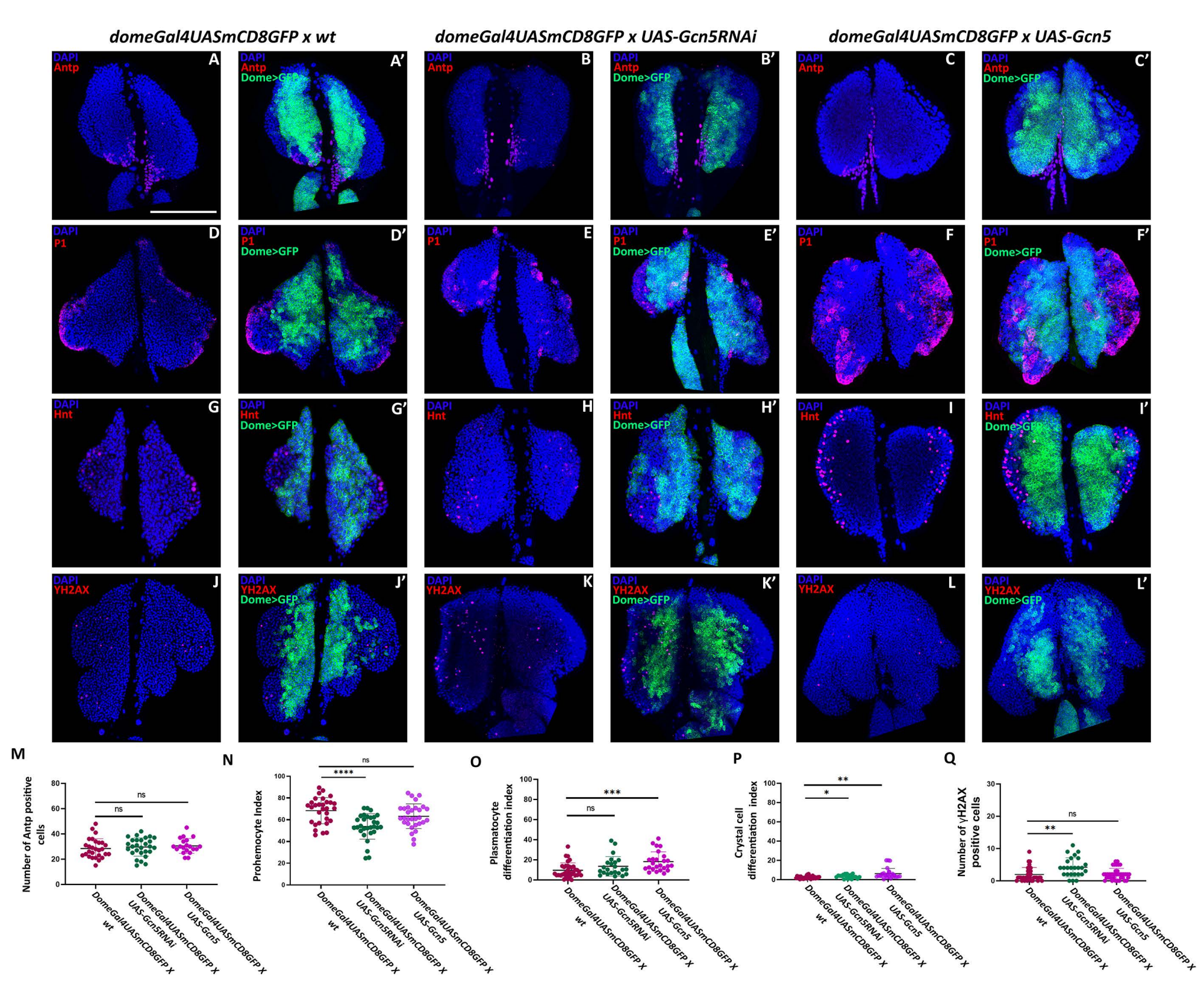
domeGal4UASmCD8GFP x wt
domeGal4UASmCD8GFP x UAS-Gcn5RNAi
domeGal4UASmCD8GFP x UAS-Gcn5
DAPI
Antp
Dome>GFP
P1
Hnt
YH2AX
A
A'
B
B'
C
C'
D
D'
E
E'
F
F'
G
G'
H
H'
I
I'
J
J'
K
K'
L
L'
M
Number of Antp positive cells
N
Prohemocyte Index
O
Plasmatocyte differentiation index
P
Crystal cell differentiation index
Q
Number of γH2AX positive cells
ns
****
***
**
*
DomeGal4UASmCD8GFP x wt
DomeGal4UASmCD8GFP x UAS-Gcn5RNAi
DomeGal4UASmCD8GFP x UAS-Gcn5

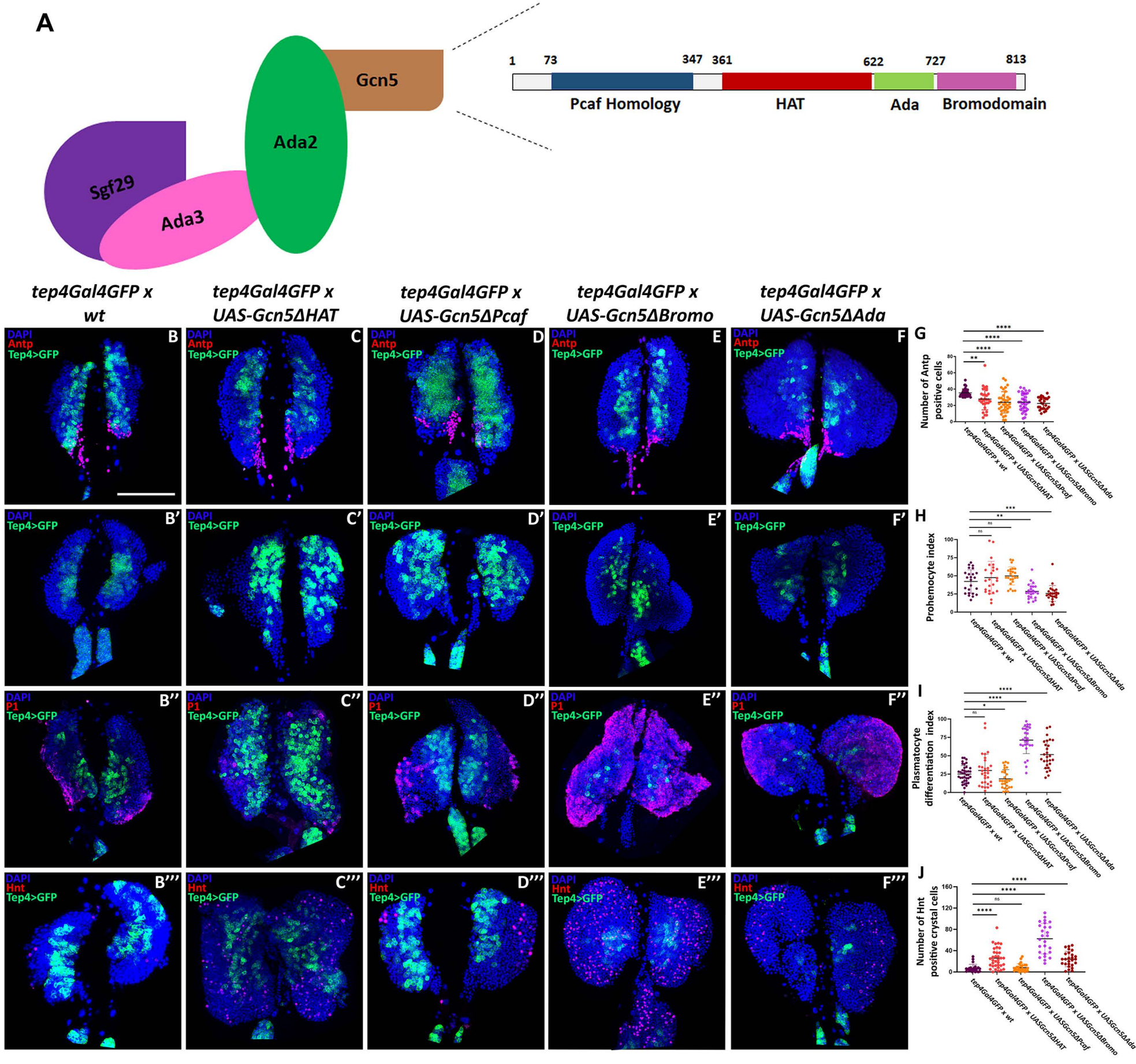
A
Gcn5
Ada2
Sgf29
Ada3
1
73
347
361
622
727
813
Pcaf Homology
HAT
Ada
Bromodomain
tep4Gal4GFP x wt
tep4Gal4GFP x UAS-Gcn5ΔHAT
tep4Gal4GFP x UAS-Gcn5ΔPcaf
tep4Gal4GFP x UAS-Gcn5ΔBromo
tep4Gal4GFP x UAS-Gcn5ΔAda
DAPI
Antp
Tep4>GFP
P1
Hnt
B
C
D
E
F
B'
C'
D'
E'
F'
B''
C''
D''
E''
F''
B'''
C'''
D'''
E'''
F'''
G
Number of Antp positive cells
H
Prohemocyte index
I
Plasmatocyte differentiation index
J
Number of Hnt positive crystal cells
tep4Gal4GFP x wt
tep4Gal4GFP x UASGcn5ΔHAT
tep4Gal4GFP x UASGcn5ΔPcaf
tep4Gal4GFP x UASGcn5ΔBromo
tep4Gal4GFP x UASGcn5ΔAda

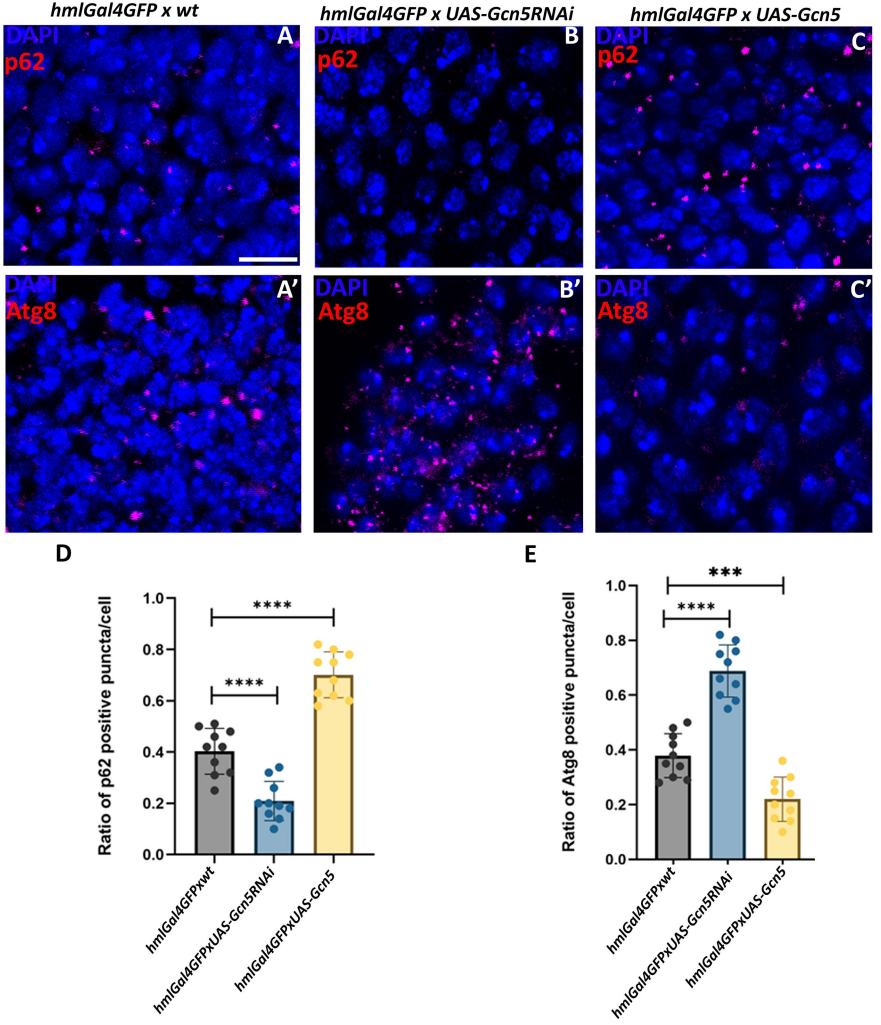
hmlGal4GFP x wt
hmlGal4GFP x UAS-Gcn5RNAi
hmlGal4GFP x UAS-Gcn5
DAPI
p62
A
B
C
Atg8
A'
B'
C'
D
E
Ratio of p62 positive puncta/cell
Ratio of Atg8 positive puncta/cell
****
***
1.0
0.8
0.6
0.4
0.2
0.0
hmlGal4GFPxwt
hmlGal4GFPxUAS-Gcn5RNAi
hmlGal4GFPxUAS-Gcn5

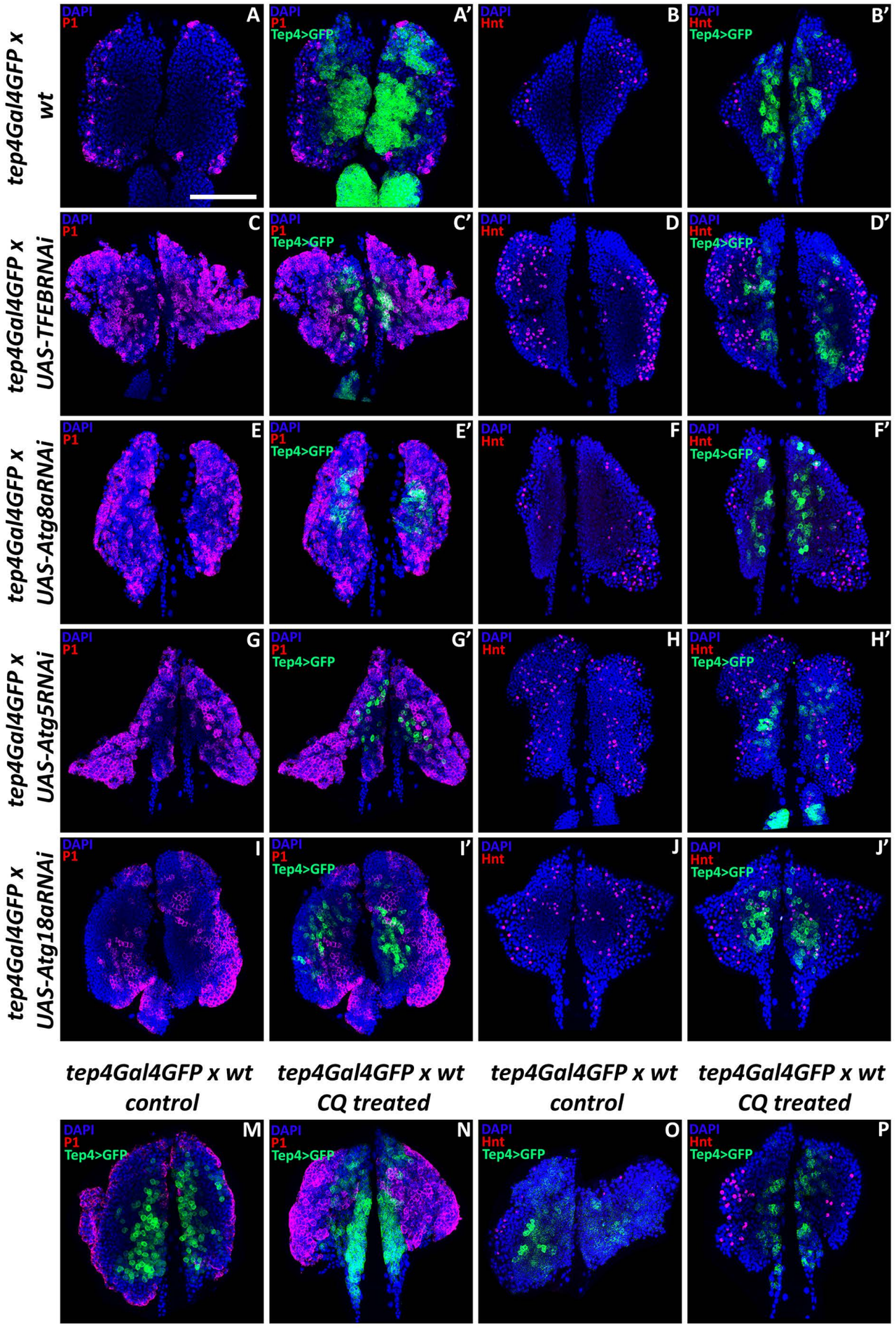
tep4Gal4GFP x wt
tep4Gal4GFP x UAS-TFEBRNAi
tep4Gal4GFP x UAS-Atg8aRNAi
tep4Gal4GFP x UAS-Atg5RNAi
tep4Gal4GFP x UAS-Atg18aRNAi
DAPI
P1
Hnt
Tep4>GFP
A
A'
B
B'
C
C'
D
D'
E
E'
F
F'
G
G'
H
H'
I
I'
J
J'
tep4Gal4GFP x wt control
tep4Gal4GFP x wt CQ treated
tep4Gal4GFP x wt control
tep4Gal4GFP x wt CQ treated
M
N
O
P

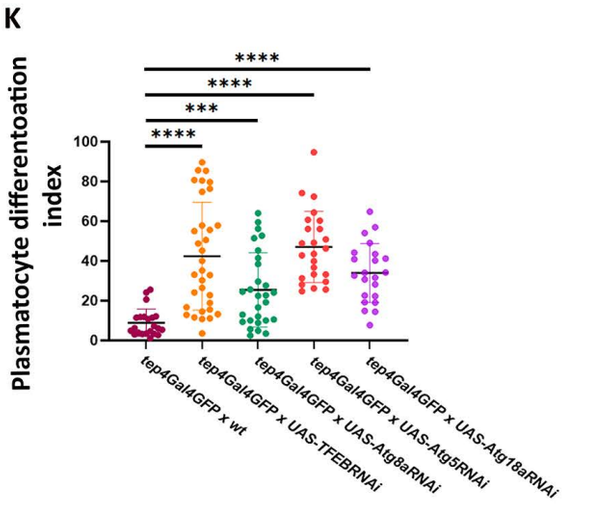
K
Plasmatocyte differentoation index
****
****
***
****
0
20
40
60
80
100
tep4Gal4GFP x wt
tep4Gal4GFP x UAS-TFEBRNAi
tep4Gal4GFP x UAS-Atg8aRNAi
tep4Gal4GFP x UAS-Atg5RNAi
tep4Gal4GFP x UAS-Atg18aRNAi

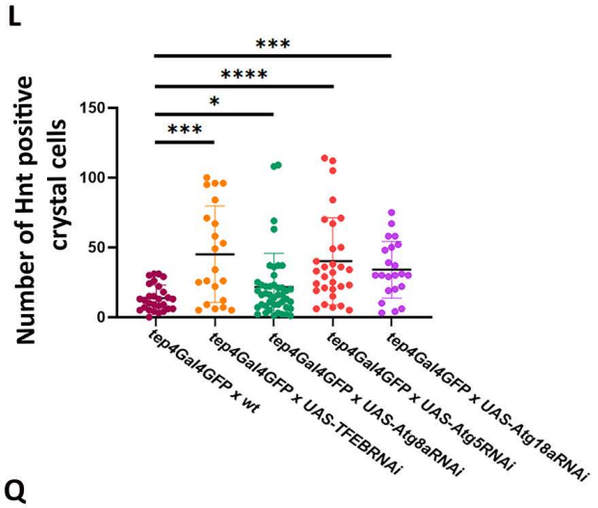
L
Number of Hnt positive crystal cells
***
****
*
***
0
50
100
150
tep4Gal4GFP x wt
tep4Gal4GFP x UAS-TFEBRNAi
tep4Gal4GFP x UAS-Atg8aRNAi
tep4Gal4GFP x UAS-Atg5RNAi
tep4Gal4GFP x UAS-Atg18aRNAi

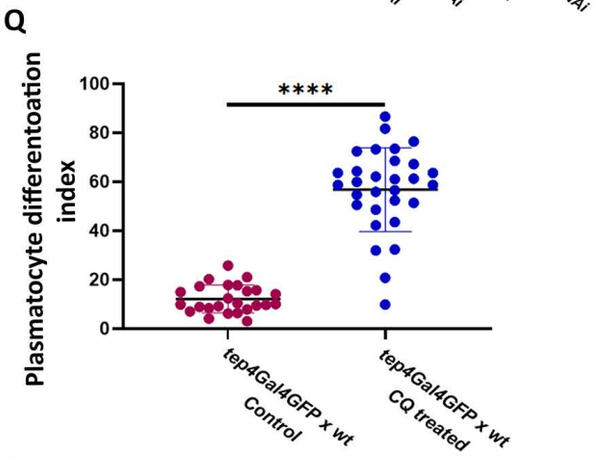
Q
Plasmatocyte differentoation index
****
0
20
40
60
80
100
tep4Gal4GFP x wt Control
tep4Gal4GFP x wt CQ treated

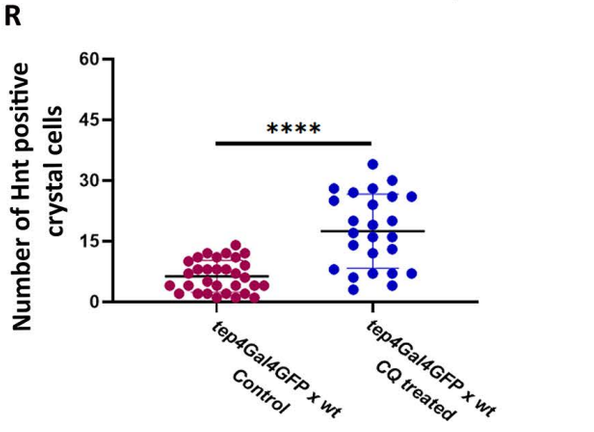
R
Number of Hnt positive crystal cells
****
0
15
30
45
60
tep4Gal4GFP x wt Control
tep4Gal4GFP x wt CQ treated

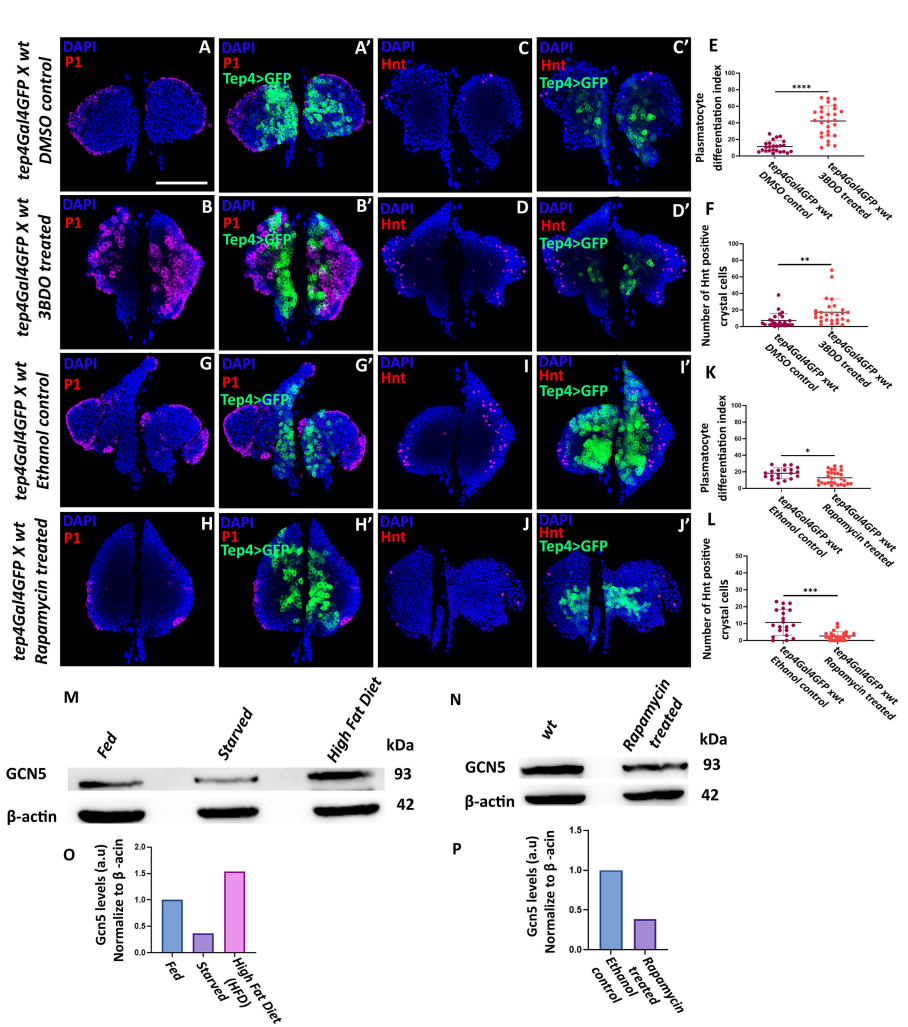
tep4Gal4GFP X wt DMSO control
tep4Gal4GFP X wt 3BDO treated
tep4Gal4GFP X wt Ethanol control
tep4Gal4GFP X wt Rapamycin treated
DAPI
P1
Hnt
Tep4>GFP
A
A'
B
B'
C
C'
D
D'
G
G'
H
H'
I
I'
J
J'
E
F
K
L
Plasmatocyte differentiation index
Number of Hnt positive crystal cells
****
**
*
***
tep4Gal4GFP xwt DMSO control
tep4Gal4GFP xwt 3BDO treated
tep4Gal4GFP xwt Ethanol control
tep4Gal4GFP xwt Rapamycin treated
M
Fed
Starved
High Fat Diet
kDa
GCN5
β-actin
93
42
N
wt
Rapamycin treated
O
Gcn5 levels (a.u) Normalize to β -acin
P
Ethanol control
Rapamycin treated

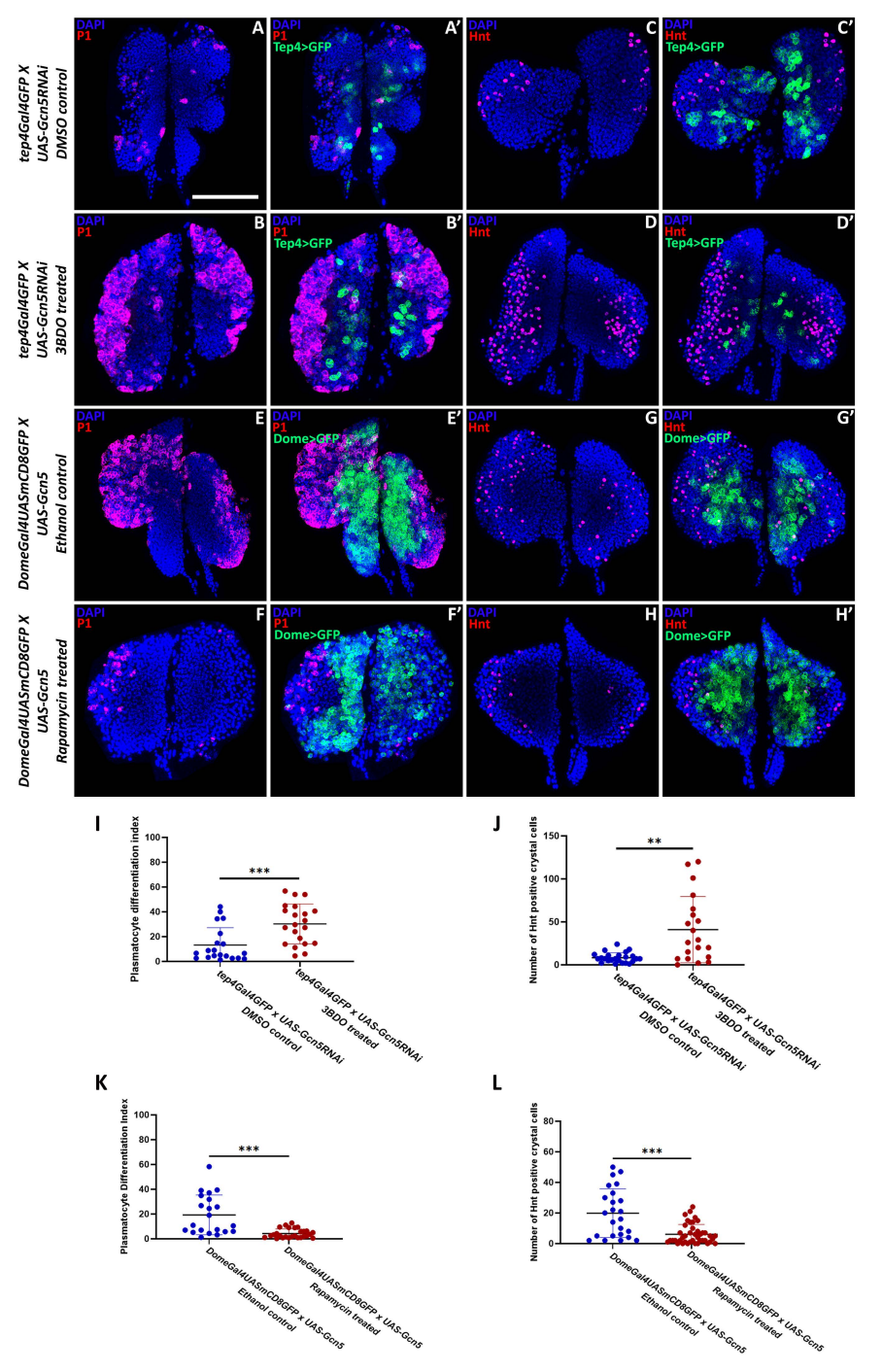
tep4Gal4GFP X UAS-Gcn5RNAi DMSO control
tep4Gal4GFP X UAS-Gcn5RNAi 3BDO treated
DomeGal4UASmCD8GFP X UAS-Gcn5 Ethanol control
DomeGal4UASmCD8GFP X UAS-Gcn5 Rapamycin treated
DAPI
P1
Tep4>GFP
Hnt
Dome>GFP
A
A'
B
B'
C
C'
D
D'
E
E'
F
F'
G
G'
H
H'
I
Plasmatocyte differentiation index
***
tep4Gal4GFP x UAS-Gcn5RNAi DMSO control
tep4Gal4GFP x UAS-Gcn5RNAi 3BDO treated
J
Number of Hnt positive crystal cells
**
K
Plasmatocyte Differentiation Index
DomeGal4UASmCD8GFP x UAS-Gcn5 Ethanol control
DomeGal4UASmCD8GFP x UAS-Gcn5 Rapamycin treated
L

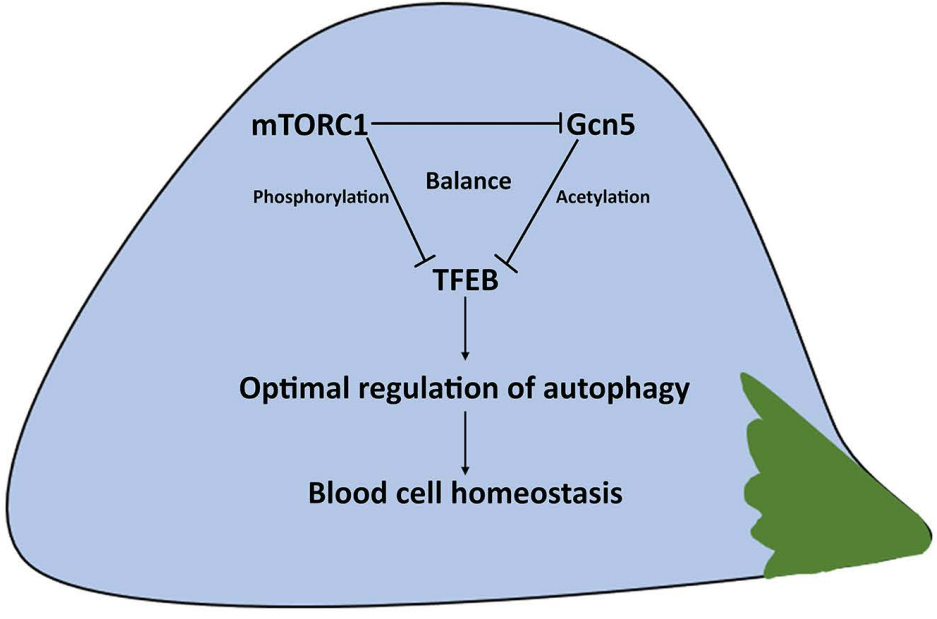

wild type

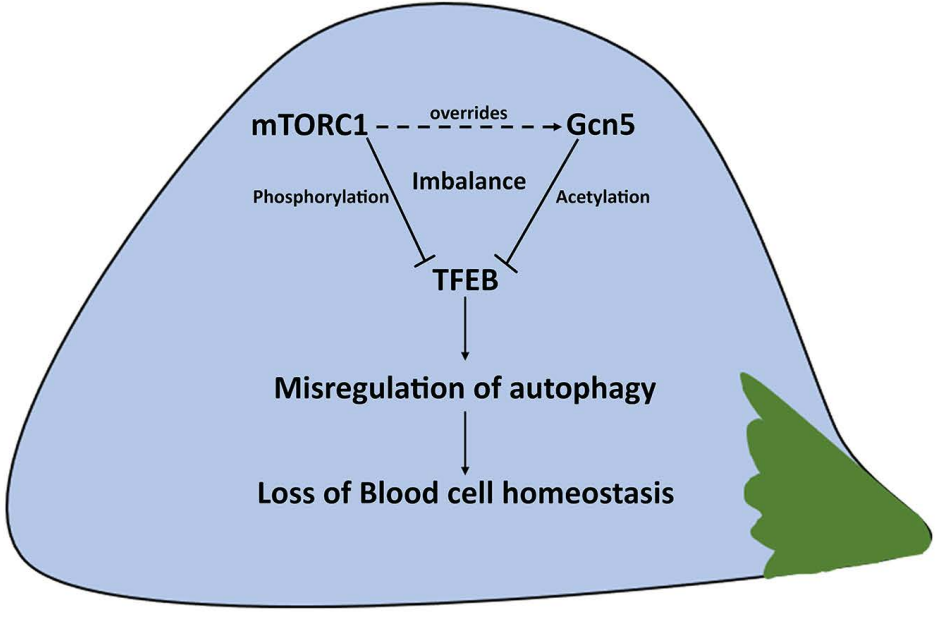

Perturbation of Gcn5-mTOR-TFEB signalling axis

Supplemental Information

Supplementary methods:

Drosophila Genetics

All the *Drosophila* stocks and crosses were maintained at 25°C, in a standard cornmeal diet. *Canton S* was used as wild type control. The fly stocks used were *gcn5E333st/TM3* (BL-9333; RRID: BDSC_9333), *gcn5C137Y/TM3* (BL-9335; RRID: BDSC_9335), UAS-Gcn5RNAi (BL-9332; RRID: BDSC_9332), *UAS-Gcn5FLAG*, *UAS-Gcn5ΔHAT*, *UAS-Gcn5ΔPcaf*, *UAS-Gcn5ΔBromo*, *UAS-Gcn5ΔAda* (Clement Carre, Sorbonne Universite, Paris), *UAS-TFEB RNAi* (Bhupendra Shravage, Agharkar Research Institute Pune, India), *UAS-Atg8aRNAi* (BL-34340; RRID:BDSC_34340), *UAS-Atg5RNAi* (BL-34899; RRID:BDSC_34899), *UAS-Atg18aRNAi* (BL-34714; RRID:BDSC_34714), *tep4Gal4GFP*, *collierGal4mCD8GFP*, *DomeGal4mCD8GFP*, *HHLTGal4GFP*, *HmlGal4GFP*, *HmldeltaGal4GFP*, *LozengeGal4Mcd8gfp* (Lucas Waltzer, Université Clermont Auvergne, France), UAS-TOR RNAi (BL-33951 RRID:BDSC 33951), UAS-raptor RNAi (BL-41912 RRID:BDSC 41912), UAS-rheb on II (gift from Mohit Prasad). *UAS-Gcn5RNAi* or *UAS-Gcn5FLAG* were crossed with tissue-specific GAL4 lines to induce Gcn5 knockdown or over-expression.

Generation of the E333st/E333st homozygous mutant:

For the generation of the *E333st/E333st* homozygous mutant, the E333st/TM3ser heterozygous mutants were crossed with *tft/cyoGFP; UG3/TM3serGFP*. The F1 (E333st/UG3) were further screened for scorable marker i.e. non-serrate phenotype and inter crossed to generate E333st/E333st homozygotes.

Antibodies

Antibodies used were mouse anti-P1 (1:100, kind gift from Dr. Istvan Ando), mouse anti-Hindsight (1:25, 1G9 – DSHB; RRID:AB_528278), mouse anti-Antp (1:25, 8C11- DSHB; RRID:AB_528083), mouse anti-γ2AX (1:400, UNC93-5.2.1 - DSHB; RRID:AB_2618077), mouse anti-DYKDDDDK Tag (anti-FLAG) (1:100, Thermo Fisher, RRID:AB_1957945), anti-P62/SQSTM1 (1:250, Proteintech, RRID:AB_10694431), anti-ATG8 (1:200, Sigma Aldrich, RRID:AB_2939040), rabbit anti-dGcn5 (1:100, gift from Clement Carre) for immunofluorescence based experiments. Normal Goat Serum (HIMEDIA, RM10701) was used as the blocking agent. Alexa-Fluor 568 conjugated secondary antibodies – Goat anti- mouse 568 (1:400, Invitrogen, RRID:AB_144696), and Goat anti-rabbit 568 (1:400, Invitrogen, RRID:AB_10563566) were used for immunofluorescence based experiments. For Western blotting, antibody concentrations used were as follows: anti-dGcn5 (1:4000), anti-p62 (1:3000), anti-ATG8 (1:4000), and anti-β-actin (1:5000). Appropriate HRP conjugated secondary antibodies – Goat anti-Mouse (Invitrogen, RRID:AB_228307) and Goat anti-Rabbit (Invitrogen, RRID:AB_228341) were used at 1:5000 concentration.

Lymph Gland Dissection and Immunohistochemistry

Wandering third instar larvae were used for lymph gland dissections as discussed in (1). The dissections were performed in phosphate buffer saline (PBS), fixed in 4% paraformaldehyde, followed by washes with PBS containing 0.3% Triton-X (PBST). The samples were then blocked in 20% normal goat serum for 20 minutes at room temperature followed by overnight primary antibody incubation at 4°C. This was followed by PBST washes, blocking, and treatment with appropriate Alexa-Flour conjugated secondary antibody incubation for two hours at room temperature. The LGs were then mounted in vectashield mounting medium containing DAPI (Vector Laboratories, RRID:AB_2336790).

Image acquisition and analysis of various Lymph Gland parameters

Confocal images were captured using either Zeiss LSM 780, Leica SP8, or Nikon AX confocal microscope. Z projection of the confocal images were used for estimating various lymph gland parameters using ImageJ/Fiji software. Plasmatocyte Differentiation Index was estimated by measuring the percentile of P1 positive area divided by the total area of the primary lobe. The Prohemocyte Index was estimated by measuring the percentile of Tep4-GFP positive area divided by the total area of primary lobe. Freehand selection tool was used for measuring the area of the plasmatocytes or the prohemocytes. For the quantification of Antp, Hnt, and γH2AX, the positive signals for respective markers were manually counted using the multi- point tool. For prohemocyte index quantitation, the GFP positive area marked by progenitors was selected, measured and it was further divided by the total area of the primary lobe. The crystal cell differentiation index was quantified by calculating the number of Hnt positive crystal cells/ total number of cells X 100. The LG quantifications were done for individual primary lymph gland lobes.

Quantification of p62 and Atg8:

Three ROIs were selected from larval LGs stained with p62 or Atg8. 5 cells per ROI were used to quantify the p62 and Atg8 positive puncta, further an average of the number of puncta per cell was quantified per ROI as the total number of positive puncta/total number of cells. These data points were further compared with the control to determine statistical significance.

Protein extraction and Western Blotting

Around 10-12 whole larvae were lysed in RIPA buffer containing protease inhibitors followed by homogenization and sonication (30s-ON, 30s-OFF x 10 cycles). The lysate was then centrifuged at 10000rpm for 5 minutes at 4°C. The supernatant was collected and quantified using BCA Protein Assay kit (Thermo Scientific, 23227) and stored at -80°C. 50µg of proteins were loaded and separated on SDS-PAGE and transferred onto a polyvinylidene difluoride (PVDF) membrane, blocked in 5% BSA for 1 hour at room temperature. The membranes were then probed with different primary antibodies. Blots were developed using an Enhanced Chemiluminescent substrate (Thermo Scientific, 34580) in Chemidoc (Bio-Rad). All the Western blotting experiments were done in biological triplicates.

Quantitative Real-Time PCR

RNA was extracted from 500 adult flies, by removing the head and perfusing the flies in cold PBS as described previously (3). The hemolymph was pelleted by centrifuging at 1500rpm for 5 minutes at 4°C. The supernatant was removed and the hemolymph pellet was lysed in TRIzol (Ambion – life technologies, 11596018). The lysates were stored at -80°C. Batches of 100 flies or more were done and once the hemolymph from all 500 flies were done, RNA was isolated by pooling all the aqueous layers post-chloroform treatment, followed by RNA isolation according to the manufacturer's protocol. RNA yield was quantified using Nanodrop. 1µg of mRNA was reverse transcribed using oligo-dT primers (Promega, C110A) and ImProm-II (Promega, A3800). Quantitation of the transcripts was done using SYBR green chemistry in Quantstudio 5 RT PCR system (Thermo Fischer Scientific). The data was analyzed using the ΔΔCt method and relative mRNA expression was normalized to rp49. Fold change calculations were done in comparison to wildtype control. The experiment was done in biological triplicates.

Chemical treatment

For drug treatments, early third instar larvae were collected and transferred to vials containing distilled water and starved for 2 hours. The larvae were then transferred to food containing corresponding drugs to be used for treatment. Chemicals used include Rapamycin (40µg/ml, R0395, Sigma-Aldrich) dissolved in absolute ethanol, 3BDO (200µM, SML1687, Sigma Aldrich) dissolved in DMSO, and Chloroquine diphosphate salt (2.5mg/ml, C6628, Sigma-Aldrich) dissolved in distilled water. For control media, post starvation, the late second instar larvae were fed on food containing respective diluents alone. For starvation experiment, the larvae were starved for 2 hours in vials containing distilled water they were then transferred to a vial containing 1ml of media mixed with chloroquine. The larvae were treated for 16 hours and were further dissected for immunostaining and then lysate was made for western blotting. For the high-fat diet experiments, the late first instar larvae were directly transferred to and reared in food containing 20% weight per volume of food-grade coconut oil. These larvae fed on a high fat diet were used for further experiments. For each of the drug treatment experiments, atleast 12 larvae were used for analysis and the treatment was done for 16 hours.

Statistical Analysis

Immunofluorescence based experiments and their analysis was performed on atleast 10 lymph glands dissected from wandering third-instar larvae. For Western Blotting and qPCR-based analysis, the experiments were done in triplicates and then analyzed. Statistical analysis was performed using the GraphPad Prism Version 9 software (RRID:SCR_002798). For analysis of statistical significance each experimental sample was tested with its respective control in a given experimental setup for all the data in each of the figures in order to estimate the P value. P values were determined by using a two-tailed unpaired Student's t-test with Welch's correction. **** indicates $p<0.0001$, *** indicates $p<0.001$, ** indicates $p<0.01$, * indicates $p<0.05$, ns (non-significant) indicates $p>0.05$. Mutant genotypes were compared to the wild- type controls and the knockdown or overexpression genotypes were compared to their respective parental Gal4 controls that were crossed to wild-type for all the statistical analysis performed. The experiments where chemical treatment has been given have been compared to the respective controls. No statistical method was used to predetermine the sample size and the experiments were not randomized. The sample size for each of the experiments has been indicated in the respective figure legends.

List of primers:

qRT primers in 5' to 3' direction

Atg1	Forward	GGCAGTGGATCGGAGAACAA
Atg1	Reverse	CATCAGCGTCTCTTCGGACA
Atg4a	Forward	TGGTTCTGTTGAAGCTGACC
Atg4a	Reverse	CCTCATTGGGTGCTCCACTT
Atg4b	Forward	TTGCACGAGTAAGTTCAAGCA
Atg4b	Reverse	CAAGGCACATGGGGTTTTGG

Atg5	Forward	AGGGAAAAGGTGCCAGTCAG
Atg5	Reverse	GATTTTTCGGTTCGGCTCGG
Atg7	Forward	CCGAAGGCGTCATCTTTGTT
Atg7	Reverse	GTTGGATACTCCGGGTCGTG
Atg9	Forward	TCAGTACCAGCAGAAGCACG
Atg9	Reverse	GCAGTGCATCACAAAGGCAA
Atg10	Forward	GGCTTGTTTCCCACGCAAAA
Atg10	Reverse	TCCGCACTGCGAGATACCTTT
Atg13	Forward	GGCGTTGCACAAATGACAGT
Atg13	Reverse	CGTTCCGCTGCATTTAGACG
Atg14	Forward	ACTGATGCTGATGCCTTTCCA
Atg14	Reverse	GCGATGGTAGACTGCTGGTT
Atg10	Forward	TAAATGCCGAGGTGGCAAGG
Atg10	Reverse	TCTGTGTGCCTGGAAGAACAA
Atg18a	Forward	GCACGCCAAGACCATGATTC
Atg18a	Reverse	TTTAGTCCCCGTCGCAGTTC

SI figure legends:

Figure S1. Blood cell homeostasis is affected in the whole animal *gcn5* heterozygous mutants.
PSC cell numbers marked by Antennapedia (red) in *gcn5[C137Y/+]* (B-B') or *gcn5[E333st/+]* (C-C') as compared to *wildtype* (A-A'). Graphical representation of PSC cell numbers of the *gcn5* mutants compared to the *wildtype* (D), n=24 for *wildtype*, n=33 for *gcn5[C137Y/+]*, and n=41 for *gcn5[E333st/+]* for PSC cell numbers quantification. Plasmatocyte differentiation was marked by P1 (red) in *gcn5[C137Y/+]* (F-F') or *gcn5[E333st/+]* (G-G') compared to the *wildtype* (E-E'). Graphical representation of plasmatocyte differentiation index of the *gcn5* heterozygous mutants compared to *wildtype* (H), n=24 for *wildtype*, n=20 for *gcn5[C137Y/+]*, and n=24 for *gcn5[E333st/+]* for quantification. Crystal cell differentiation marked by Hnt (red) in *gcn5[C137Y/+]* (J-J') or *gcn5[E333st/+]* (K-K') compared to *wildtype* (I-I'). Graphical representation of the number of Crystal cells for *gcn5* heterozygous mutants compared to *wildtype* (L), n=26 for *wildtype*, n=26 for *gcn5[C137Y/+]*, and n=23 for *gcn5[E333st/+]* for quantification. Cells undergoing DNA damage marked by γH2AX (red) in *gcn5[C137Y/+]* (N-N') or *gcn5[E333st/+]* (O-O') as compared to *wildtype* (M-M'). Graphical representation of γH2AX marked DNA damage of the heterozygous *gcn5* mutants compared to the *wildtype* (P), n=31 for *wildtype*, n=42 for *gcn5[C137Y/+]*, and n=28 for *gcn5[E333st/+]* for quantification. Nuclei are stained with DAPI (Blue). n represents the number of individual primary lobes of the LG. Individual data points in the graphs represent individual primary lobes of the LG. Values are mean ± SD, and asterisk marks statistically significant differences (*$p<0.05$; **$p<0.01$; ****$p<0.0001$, Student's t-test with Welch's correction). Scale Bar: 50µm (A-O').

Figure S2. Validation of Gcn5 knockdown and over-expression constructs
Gcn5 (red) expression upon Hml-Gal4 mediated Gcn5 knockdown (B-B') or over-expression (C-C') in the hml population, compared to wildtype (A-A'). FLAG (red) expression upon Gcn5 over-expression (E-E') in the hml population, compared to wildtype (D-D'). Nuclei are stained with DAPI (Blue). Scale Bar: 50µm (A-E').

Figure S3. Collier mediated modulation of Gcn5 levels in the PSC alters LG homeostasis.
PSC cell population marked by Antennapedia (red) upon knockdown (B-B') or over-expression (C-C') of Gcn5 in the Collier population (green) compared to wildtype (A-A'). Plasmatocyte differentiation marked by P1 (red) upon knockdown (E-E') or over-expression (F-F') of Gcn5 in the Collier population (green) compared to wildtype (D-D'). Crystal cell differentiation marked by Hnt (red) upon knockdown (H-H') or over-expression (I-I') of Gcn5 in the Collier population (green) compared to wild type (G-G'). Cells undergoing DNA damage marked by γH2AX (red) upon knockdown (K-K') or over-expression (L-L') of Gcn5 in the Collier population (green) compared to wild type (J-J'). Graphical representation of PSC cell numbers upon modulation of Gcn5 levels in the Collier population compared to wildtype (M), n=21 for wildtype, n=29 for Gcn5 knockdown, and n=22 for Gcn5 over-expression. Graphical representation of plasmatocyte differentiation Index upon modulation of Gcn5 levels in Collier population compared to wildtype (N), n=23 for wildtype, n=23 for Gcn5 knockdown, and n=20 for Gcn5 over-expression. Graphical representation of numbers of Crystal cells upon modulation of Gcn5 levels in the Collier population compared to wildtype (O), n=22 for wildtype, n=21 for Gcn5 knockdown, and n=24 for Gcn5 over-expression. Graphical representation of γH2AX positive cells upon modulation of Gcn5 levels in the Collier population compared to wildtype (P), n=29 for wildtype, n=27 for Gcn5 knockdown, and n=21 for Gcn5 over-expression. Nuclei are stained with DAPI (blue). PSC cell specific Gcn5

modulation was performed using Collier-Gal4. n represent the number of individual primary lobes of the LG. Individual data points in the graphs represent individual primary lobes of the LG. Values are mean ± SD, and asterisk marks statistically significant differences (*p<0.05; **p<0.01; ***p<0.001, Student's t-test with Welch's correction). Scale Bar: 50µm (A-L')

Figure S4. HmlΔ mediated modulation of Gcn5 levels in the differentiated blood cell population results in altered hematopoiesis.

PSC cell population marked by Antennapedia (red) upon knockdown (B-B') or over-expression (C-C') of Gcn5 in the HmlΔ population (green) compared to wildtype (A-A'). Plasmatocyte differentiation marked by P1 (red) upon knockdown (E-E') or over-expression (F-F') of Gcn5 in the HmlΔ population (green) compared to wildtype (D-D'). Crystal cell differentiation marked by Hnt (red) upon knockdown (H-H') or over-expression (I-I') of Gcn5 in the HmlΔ population (green) compared to wildtype (G-G'). Cells undergoing DNA damage marked by γH2AX (red) upon knockdown (K-K') or over-expression (L-L') of Gcn5 in the HmlΔ population (green) compared to wildtype (J-J'). Graphical representation of PSC cell numbers upon modulation of Gcn5 levels in the HmlΔ population compared to wildtype (M), n=24 for wildtype, n=25 for Gcn5 knockdown, and n=36 for Gcn5 over-expression. Graphical representation of plasmatocyte differentiation Index upon modulation of Gcn5 levels in HmlΔ population compared to wildtype (N), n=20 for wildtype, n=20 for Gcn5 knockdown, and n=21 for Gcn5 over-expression. Graphical representation of numbers of Crystal cells upon modulation of Gcn5 levels in the HmlΔ population compared to wildtype (O), n=25 for wildtype, n=21 for Gcn5 knockdown, and n=22 for Gcn5 over-expression. Graphical representation of γH2AX positive cells upon modulation of Gcn5 levels in the HmlΔ population compared to wildtype (P), n=23 for wildtype, n=29 for Gcn5 knockdown, and n=27 for Gcn5 over-expression. Nuclei are stained with DAPI (blue). HmlΔ-Gal4 was used for differentiated blood cells specific Gcn5 modulation. n represent the number of individual primary lobes of the LG. Individual data points in the graphs represent individual primary lobes of the LG. Values are mean ± SD, and asterisk marks statistically significant differences (*p<0.05; ***p<0.001; ****p<0.0001, Student's t-test with Welch's correction). Scale Bar: 50µm (A-L').

Figure S5: GCN5 positively regulates crystal cell differentiation cell-autonomously

GCN5 (magenta) expression in lz-GFP (Green) positive crystal cells in larval LGs where lz-Gal4 drives UAS-GFP in wild type genetic background (A-B). Crystal cell differentiation marked by Hindsight (Hnt, magenta) upon GCN5 over-expression using lz- Gal4GFP (D) as compared to control (C) and quantitated as total number of crystal cells per LG lobe represented by n, where n=31 for wildtype and n=36 for GCN5 overexpression. (G). GCN5 (magenta) expression in posterior LG lobes marked by GFP (Green) driven by tep4- Gal4 (E-F). Nuclei = DAPI (Blue) and GFP driven by either lz-Gal4 or tep4-Gal4. Values are mean ± SD, and asterisk marks statistically significant differences with *** as p<0.001 analyzed by Student's t- test with Welch's correction. Scale Bar: 30µm (A-B), 50 µm (C-F).

Figure S6. Prohemocyte-specific expression of Gcn5 domain deletion constructs leads to increased DNA damage.

Cells undergoing DNA damage marked by γH2AX (red) upon expression of different Gcn5 domain deletion constructs in the tep-GFP population using tep4-Gal4 (green) (B-E') as compared to wildtype (A, A'). Graphical representation of Cells undergoing DNA damage marked by γH2AX (F), where n=27 for wildtype, n=26 for Gcn5ΔHAT expression, n=27 for Gcn5ΔPcaf expression, n=23 for Gcn5ΔBromo expression, and n=25 for Gcn5ΔAda expression in the tep population. Nuclei are stained with DAPI (blue). n represents the number of individual primary lobes of the LG. Individual data points in the graphs represent individual

primary lobes of the LG. Values are mean ± SD, and asterisk marks statistically significant differences (**p<0.01; ***p<0.001; ****p<0.0001, Student's t-test with Welch's correction). Scale Bar: 50µm (A-E')

Figure S7. Gcn5 over-expression leads to suppression of autophagy-related genes
Transcript levels of different autophagy effector genes in Hml-Gal4 mediated Gcn5 over-expression genetic background as compared to the Hml-Gal4 X wt control. rp49 was used as an endogenous control to normalize the mRNA expression.

Figure S8: Prohemocyte- specific genetic abrogation of autophagy affects the niche cell numbers and induces DNA damage.
PSC/niche cells marked by Antennapedia (red) upon tep4-Gal4 mediated knockdown of TFEB (C-C'), Atg8a (E-E'), Atg5 (G-G'), or Atg18 (I-I') in the tep population (green) as compared to wildtype (A-A'). DNA damage marked by Gamma-H2Ax (red) upon tep4-Gal4 mediated knockdown of TFEB (D-D'), Atg8a (F-F'), Atg5 (H-H'), or Atg18 (J-J') in the tep population (green) as compared to wildtype (B-B'). Graphical representation of niche cell numbers upon knockdown of TFEB (n=40), Atg8a (n=36), Atg5 (n=39), Atg18 (n=41) in the tep population, compared to the wildtype (n=33) (K). Graphical representation of Gamma-H2Ax positive foci upon knockdown of TFEB (n=37), Atg8a (n=34 , Atg5 (n=33), or Atg18 (n=36) in the tep population, compared to the wildtype (n=35) (L). Graphical representation of prohemocyte index upon knockdown of TFEB (n=30), Atg8a (n=30), Atg5 (n=30), Atg18 (n=30) in the tep population, compared to the wildtype (n=33) (M). Nuclei are stained with DAPI (blue). n represents the number of individual primary lobes of the LG. Individual data points in the graphs represent individual primary lobes of the LG. Values are mean ± SD, and asterisk marks statistically significant differences (*p<0.05; ***p<0.001; ****p<0.0001, Student's t- test with Welch's correction). Scale Bar: 50µm (A-J')

Figure S9: Autophagy levels in the LG hemocytes are affected upon systemic Chloroquine treatment
Chloroquine treated tep4-Gal4GFP X wt larvae expressing GFP (Green) driven by tep4-Gal4 showing p62 or Atg8 positive puncta (magenta) in LG hemocytes (B-B', D-D') as compared to vehicle treated (A-A', C-C') and represented as number of p62 or Atg8 positive puncta per cell (n),where n= 255 cells for vehicle treated and n=300 cells for chloroquine treated p62 positive cells and n= 360 cells for vehicle treated and n= 390 cells for chloroquine treated Atg8 positive cells respectively.(E and F). Nuclei = DAPI (Blue) and GFP driven by tep4-Gal4. Values are mean ± SD, and asterisk marks statistically significant differences with **** as p<0.0001 analyzed by Student's t- test with Welch's correction. Scale Bar: 30µm (A-D')

Figure S10: Genetic modulation of mTORC1 activity in the hematopoietic progenitors regulates blood cell differentiation
Plasmatocyte differentiation marked by P1 (magenta) upon tep4-Gal4 mediated depletion of tor (B) or raptor (C) or over-expression of Rheb (D) as compared to the wild type control (A) quantitated as plasmatocyte differentiation index per LG lobe where n represents the number of primary lobes of LG, n= 45 for wildtype, n= 39 for tor knockdown, n= 43 for raptor knockdown and n=44 for Rheb overexpression. (I). Crystal cell differentiation marked by Hindsight (Hnt, magenta) upon tep4-Gal4 mediated depletion of tor (F) or raptor (G) or over-expression of Rheb (H) as compared to the wild type control (E) quantitated as crystal cell differentiation index per LG lobe(n), where n represents the number of primary lobes of LG, n= 31 for wildtype, n= 42 for tor knockdown, n=30 for raptor knockdown, n=28 for Rheb overexpression. (J). Nuclei = DAPI (Blue) and GFP is driven by tep4-Gal4. n = number of individual primary lobes of the LG. Individual data points in the graphs represent individual

primary lobes of the LG. Values are mean ± SD, and asterisk marks statistically significant differences (*p<0.05; ***p<0.001; ****p<0.0001, ns = non-significant. Student's t- test with Welch's correction). Scale Bar: 50µm (A-H)

Figure S11: Genetic modulation of mTORC1 activity in the hematopoietic progenitors alters niche cell numbers and causes DNA damage

PSC/niche cell numbers marked by Antennapedia (Antp, magenta) upon tep4-Gal4 mediated depletion of tor (B) or raptor (C) or over-expression of Rheb (D) as compared to the wild type control (A) quantitated as Antp positive niche cell numbers per LG lobe represented by n, where n= 38 for wildtype, n= 37 for tor knockdown, n=42 for raptor knockdown, n=37 for Rheb overexpression. (I). γ-H2Ax foci positive cells showing DNA damage (magenta) upon tep4-Gal4 mediated depletion of tor (F) or raptor (G) or over-expression of Rheb (H) as compared to the wild type control (E) quantitated as total number of γ-H2Ax positive foci per LG lobe represented by n, where n= 40 for wildtype, n= 43 for tor knockdown, n=34 for raptor knockdown, n=37 for Rheb overexpression. (J). Nuclei = DAPI (Blue) and GFP is driven by tep4-Gal4. n = number of individual primary lobes of the LG. Individual data points in the graphs represent individual primary lobes of the LG. Values are mean ± SD, and asterisk marks statistically significant differences (*p<0.05; ***p<0.001; ****p<0.0001, ns = non-significant. Student's t- test with Welch's correction). Scale Bar: 50µm (A-H)

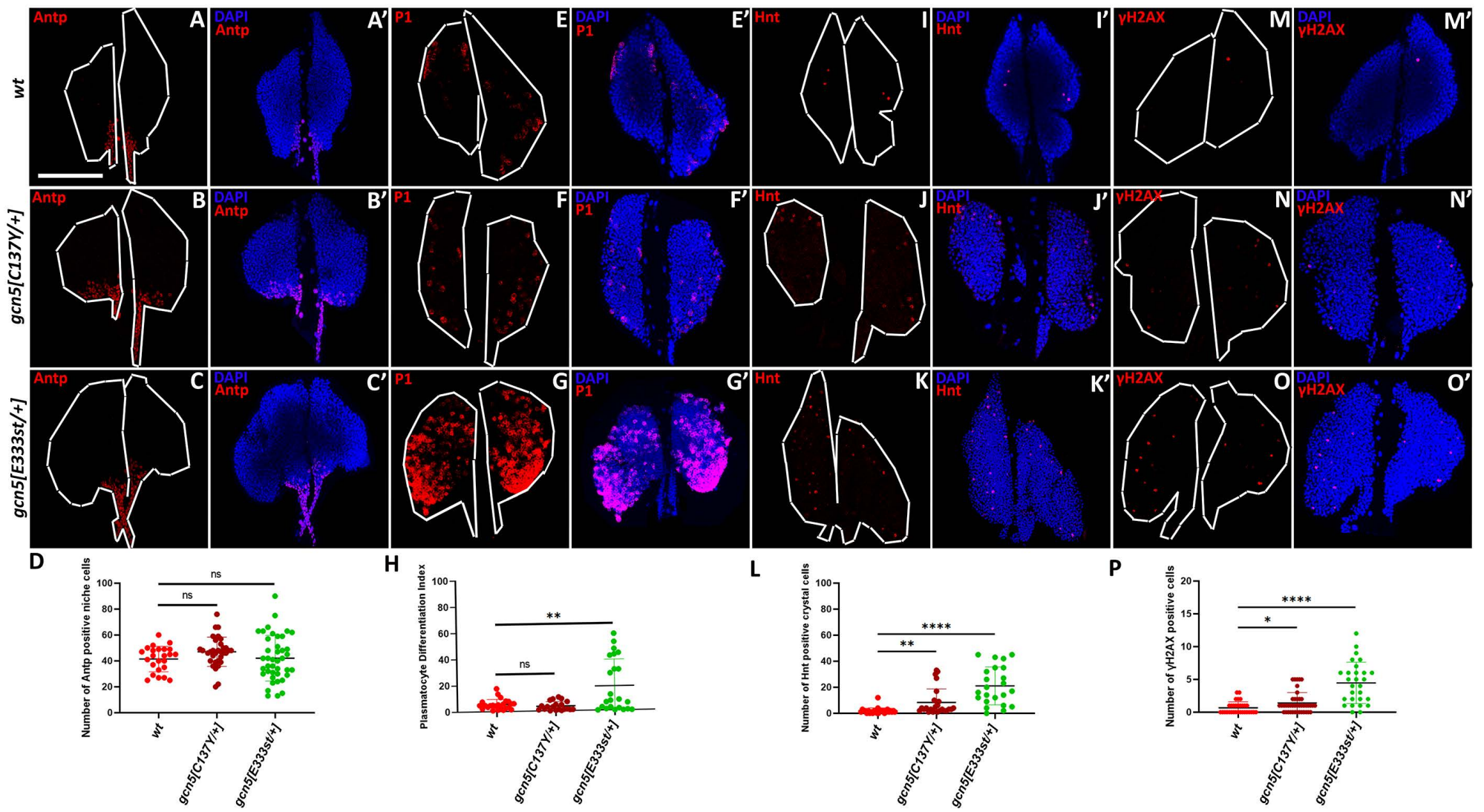
wt
gcn5[C137Y/+]
gcn5[E333st/+]
Antp
DAPI
P1
Hnt
γH2AX
A
A'
B
B'
C
C'
E
E'
F
F'
G
G'
I
I'
J
J'
K
K'
M
M'
N
N'
O
O'
D
Number of Antp positive niche cells
ns
H
Plasmatocyte Differentiation Index
**
L
Number of Hnt positive crystal cells
****
P
Number of γH2AX positive cells
*

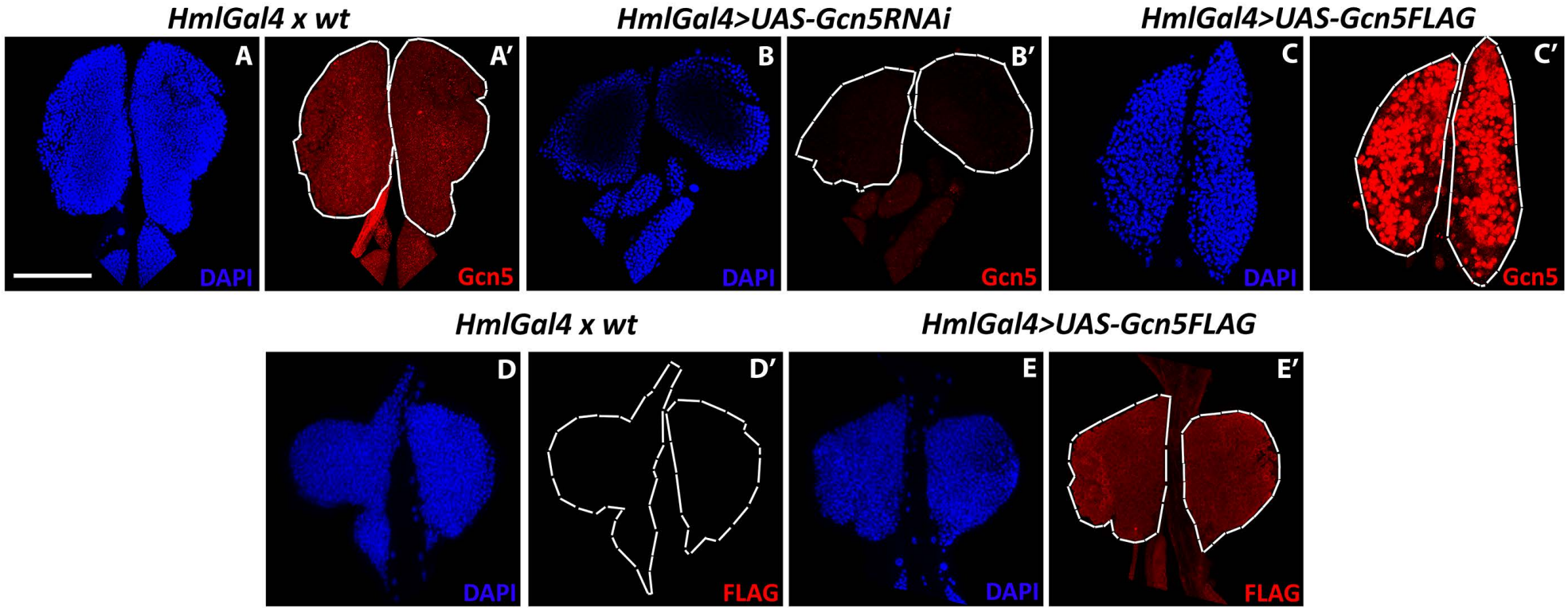
HmlGal4 x wt
HmlGal4>UAS-Gcn5RNAi
HmlGal4>UAS-Gcn5FLAG
A
A′
B
B′
C
C′
DAPI
Gcn5
DAPI
Gcn5
DAPI
Gcn5
HmlGal4 x wt
HmlGal4>UAS-Gcn5FLAG
D
D′
E
E′
DAPI
FLAG
DAPI
FLAG

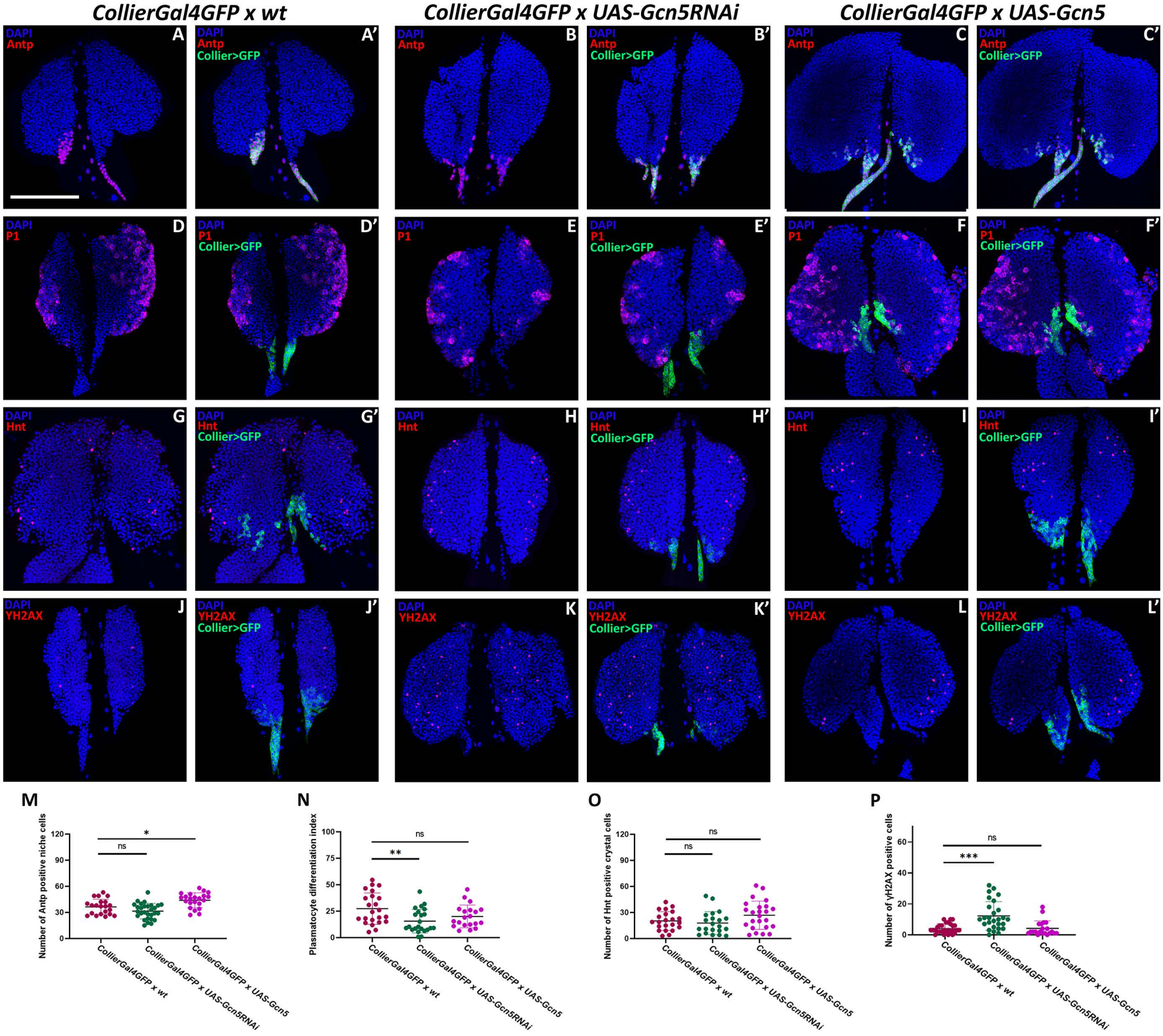
CollierGal4GFP x wt
CollierGal4GFP x UAS-Gcn5RNAi
CollierGal4GFP x UAS-Gcn5
A
A'
B
B'
C
C'
D
D'
E
E'
F
F'
G
G'
H
H'
I
I'
J
J'
K
K'
L
L'
DAPI
Antp
P1
Hnt
YH2AX
Collier>GFP
M
N
O
P
Number of Antp positive niche cells
Plasmatocyte differentiation index
Number of Hnt positive crystal cells
Number of γH2AX positive cells
ns
*
**
***
CollierGal4GFP x wt
CollierGal4GFP x UAS-Gcn5RNAi
CollierGal4GFP x UAS-Gcn5

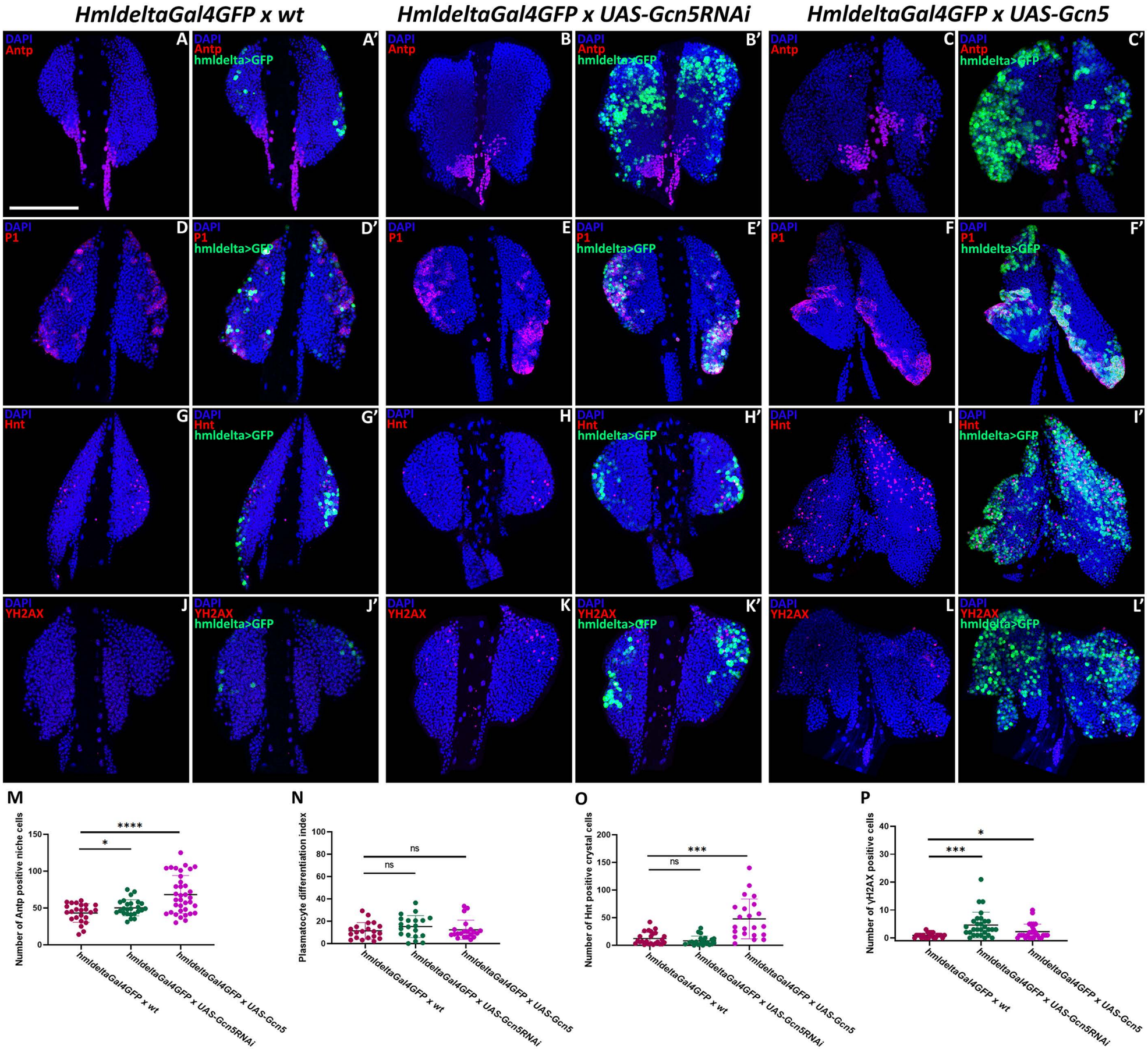
HmldeltaGal4GFP x wt
HmldeltaGal4GFP x UAS-Gcn5RNAi
HmldeltaGal4GFP x UAS-Gcn5
DAPI
Antp
P1
Hnt
YH2AX
hmldelta>GFP
A
A'
B
B'
C
C'
D
D'
E
E'
F
F'
G
G'
H
H'
I
I'
J
J'
K
K'
L
L'
M
Number of Antp positive niche cells
N
Plasmatocyte differentiation index
O
Number of Hnt positive crystal cells
P
Number of γH2AX positive cells
ns
*
**
***
****
hmldeltaGal4GFP x wt
hmldeltaGal4GFP x UAS-Gcn5RNAi
hmldeltaGal4GFP x UAS-Gcn5

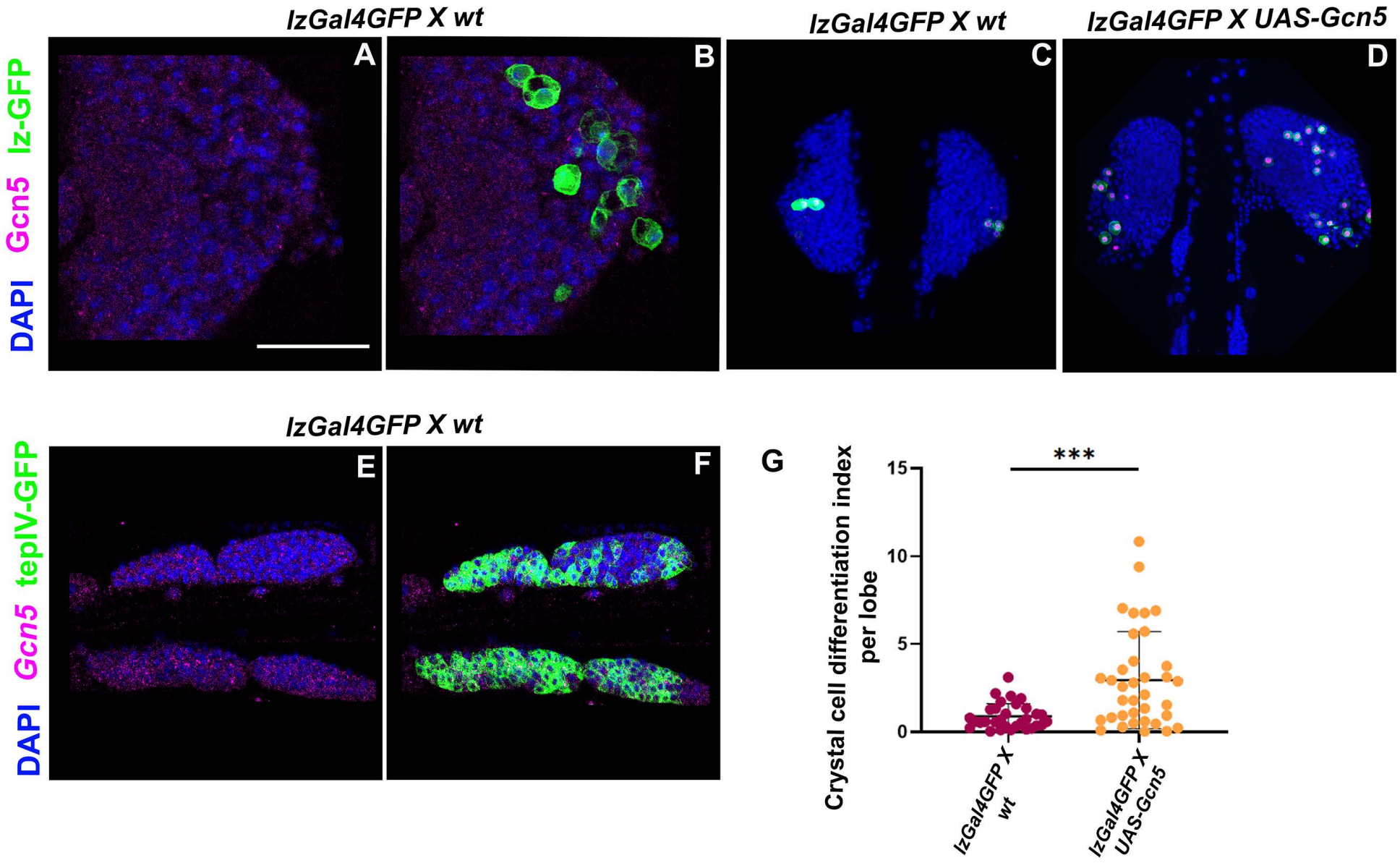
lzGal4GFP X wt
lzGal4GFP X wt
lzGal4GFP X UAS-Gcn5
A
B
C
D
lz-GFP
Gcn5
DAPI
lzGal4GFP X wt
E
F
tepIV-GFP
Gcn5
DAPI
G
***
Crystal cell differentiation index per lobe
15
10
5
0
lzGal4GFP X wt
lzGal4GFP X UAS-Gcn5

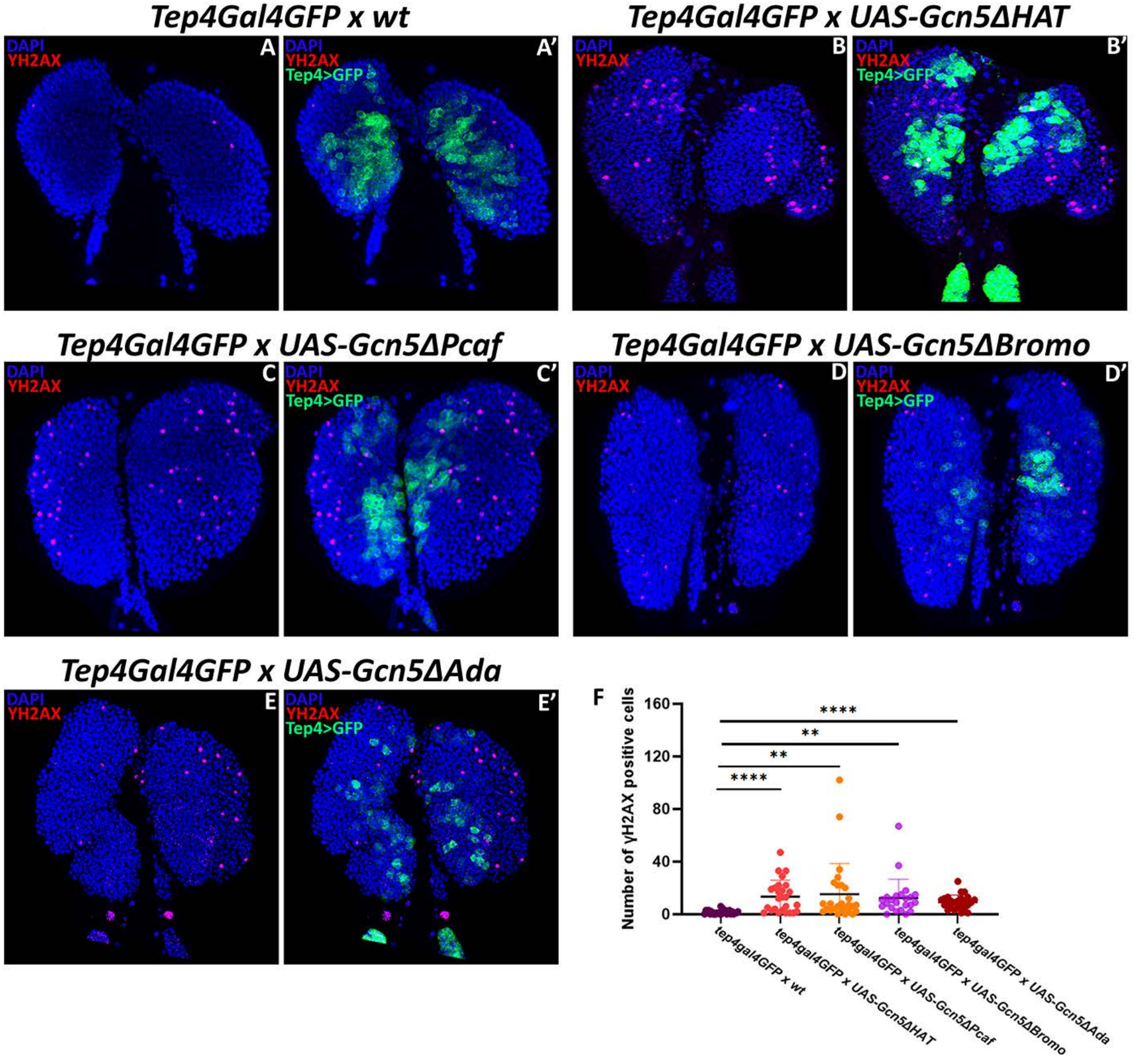
Tep4Gal4GFP x wt
Tep4Gal4GFP x UAS-Gcn5ΔHAT
Tep4Gal4GFP x UAS-Gcn5ΔPcaf
Tep4Gal4GFP x UAS-Gcn5ΔBromo
Tep4Gal4GFP x UAS-Gcn5ΔAda
DAPI
YH2AX
Tep4>GFP
A
A'
B
B'
C
C'
D
D'
E
E'
F
Number of γH2AX positive cells
160
120
80
40
0
****
**
**
****
tep4gal4GFP x wt
tep4gal4GFP x UAS-Gcn5ΔHAT
tep4gal4GFP x UAS-Gcn5ΔPcaf
tep4gal4GFP x UAS-Gcn5ΔBromo
tep4gal4GFP x UAS-Gcn5ΔAda

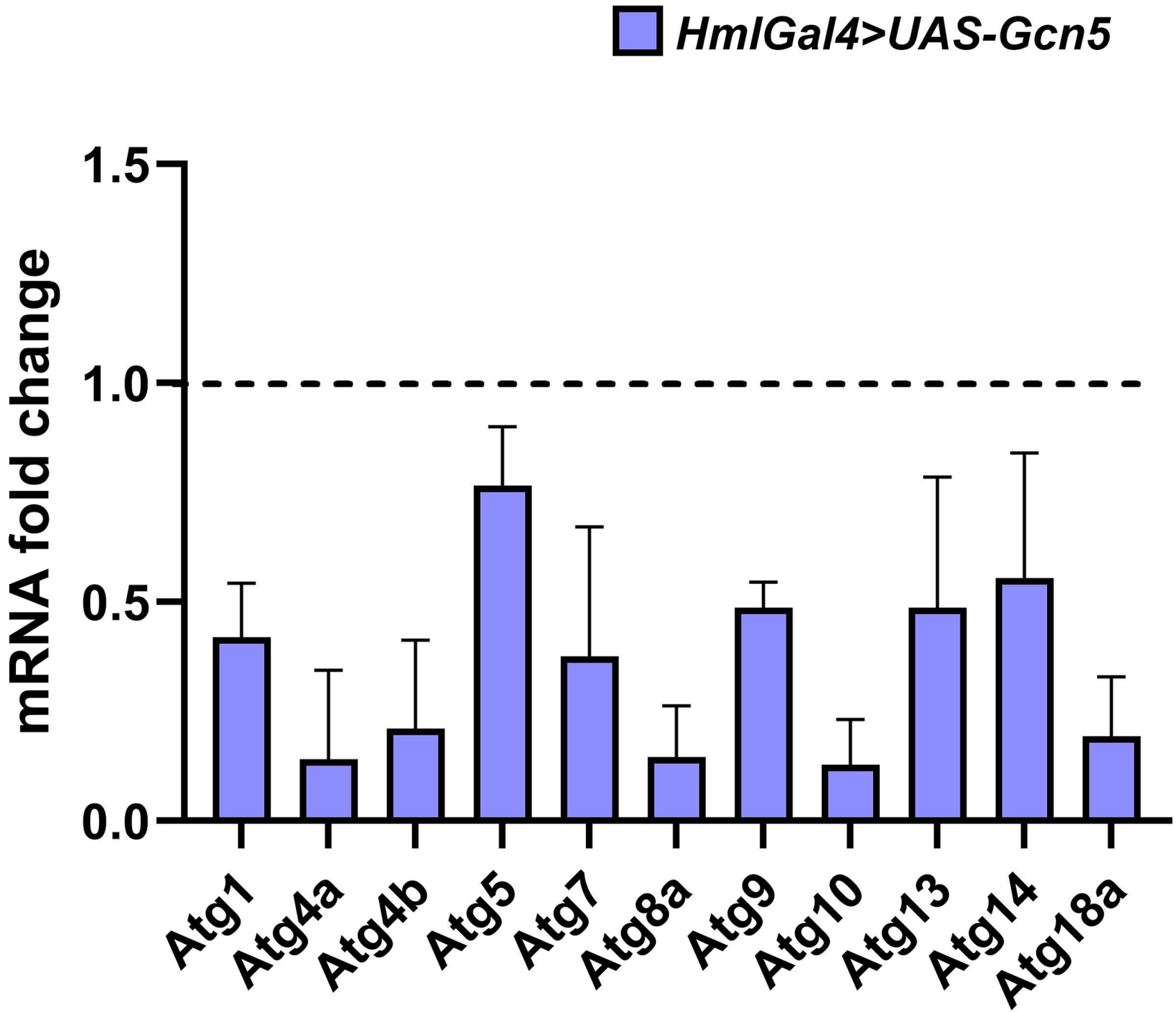
HmlGal4>UAS-Gcn5
mRNA fold change
1.5
1.0
0.5
0.0
Atg1
Atg4a
Atg4b
Atg5
Atg7
Atg8a
Atg9
Atg10
Atg13
Atg14
Atg18a

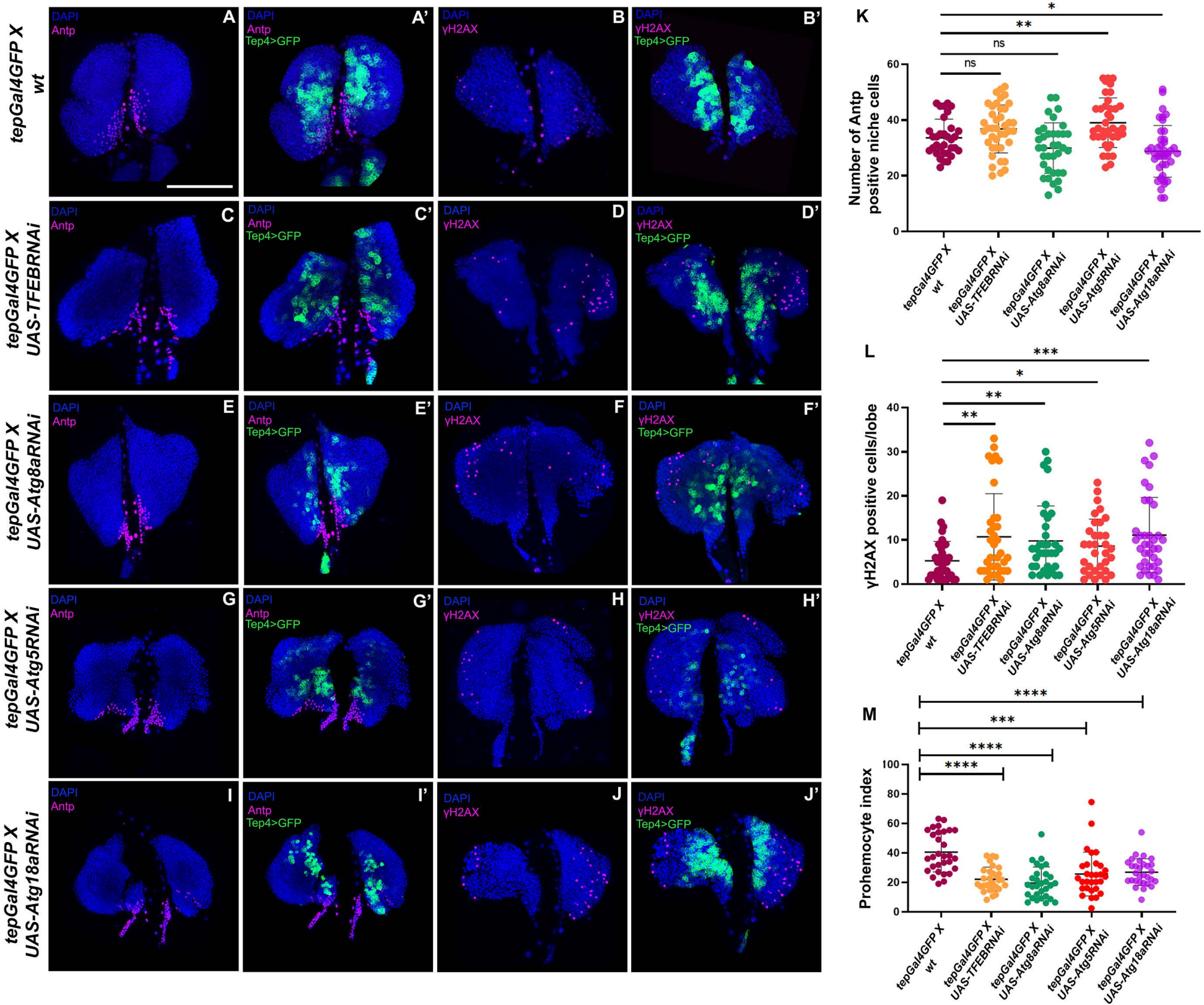
tepGal4GFP X wt
tepGal4GFP X UAS-TFEBRNAi
tepGal4GFP X UAS-Atg8aRNAi
tepGal4GFP X UAS-Atg5RNAi
tepGal4GFP X UAS-Atg18aRNAi
DAPI
Antp
Tep4>GFP
γH2AX
A
A'
B
B'
C
C'
D
D'
E
E'
F
F'
G
G'
H
H'
I
I'
J
J'
K
Number of Antp positive niche cells
ns
ns
**
*
L
γH2AX positive cells/lobe
**
**
*
***
M
Prohemocyte index
****
****
***
****

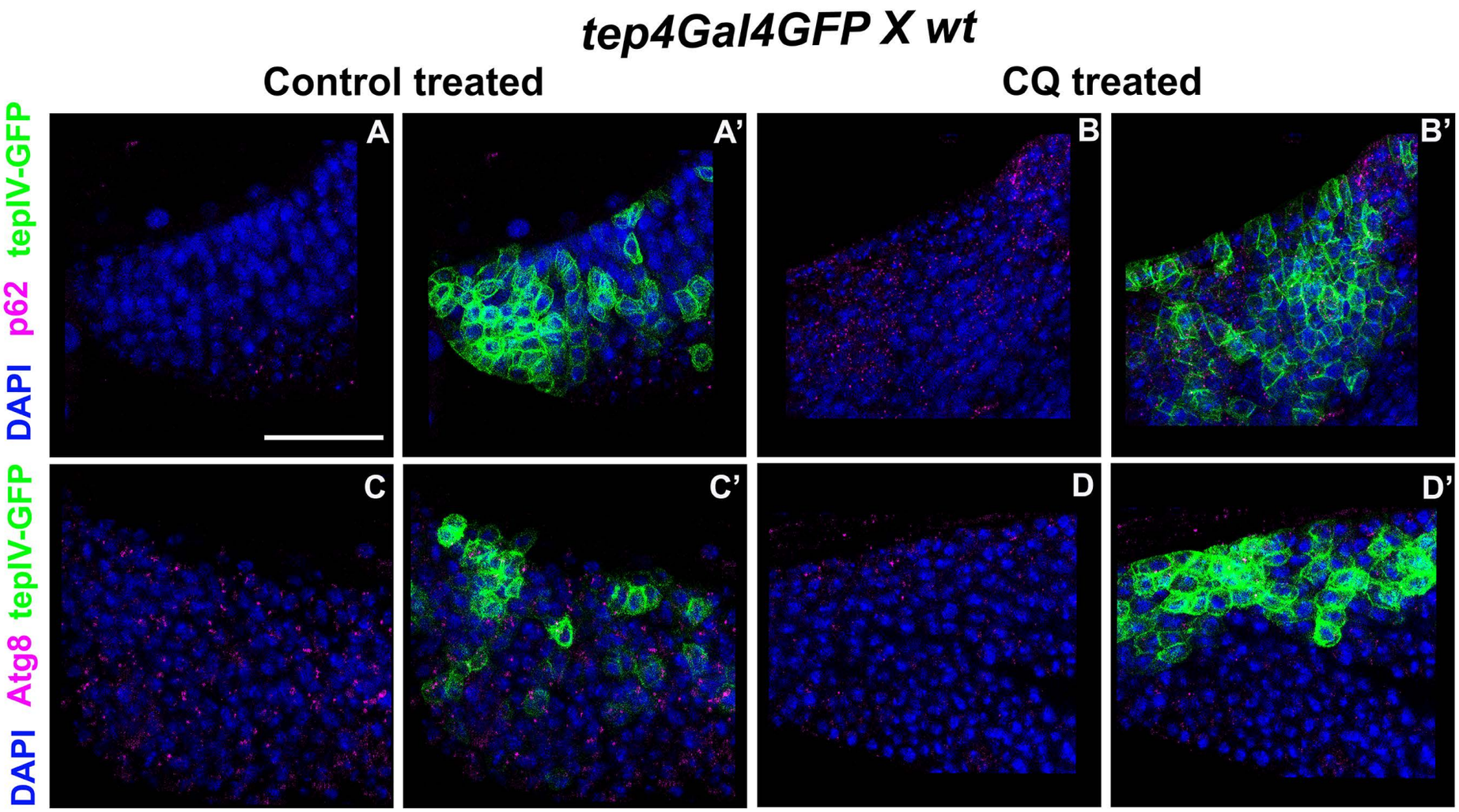
tep4Gal4GFP X wt
Control treated
CQ treated
tepIV-GFP
p62
DAPI
Atg8
A
A'
B
B'
C
C'
D
D'

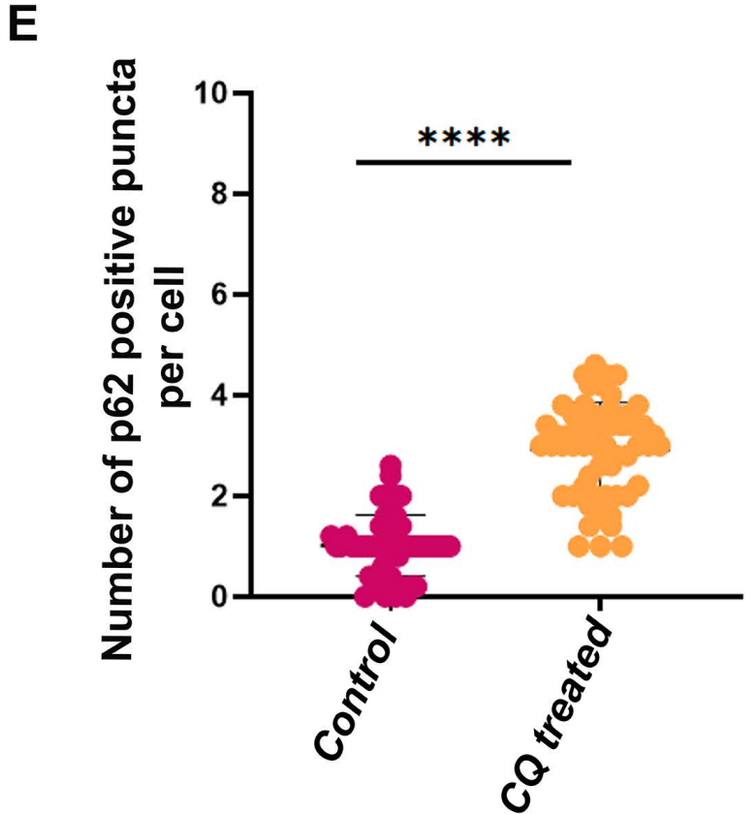
E
Number of p62 positive puncta per cell
****
Control
CQ treated

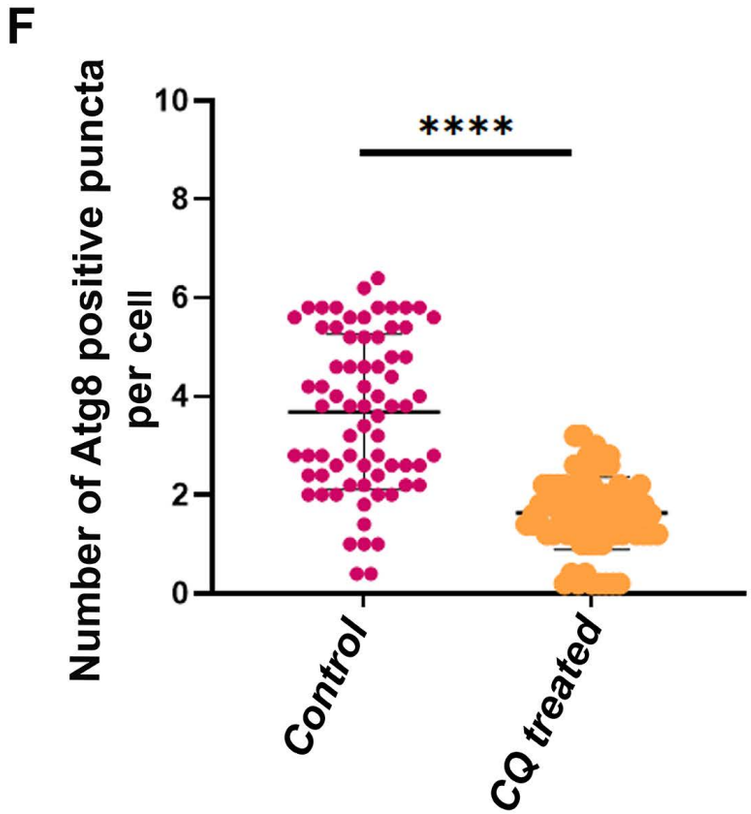
F
Number of Atg8 positive puncta per cell
****
Control
CQ treated

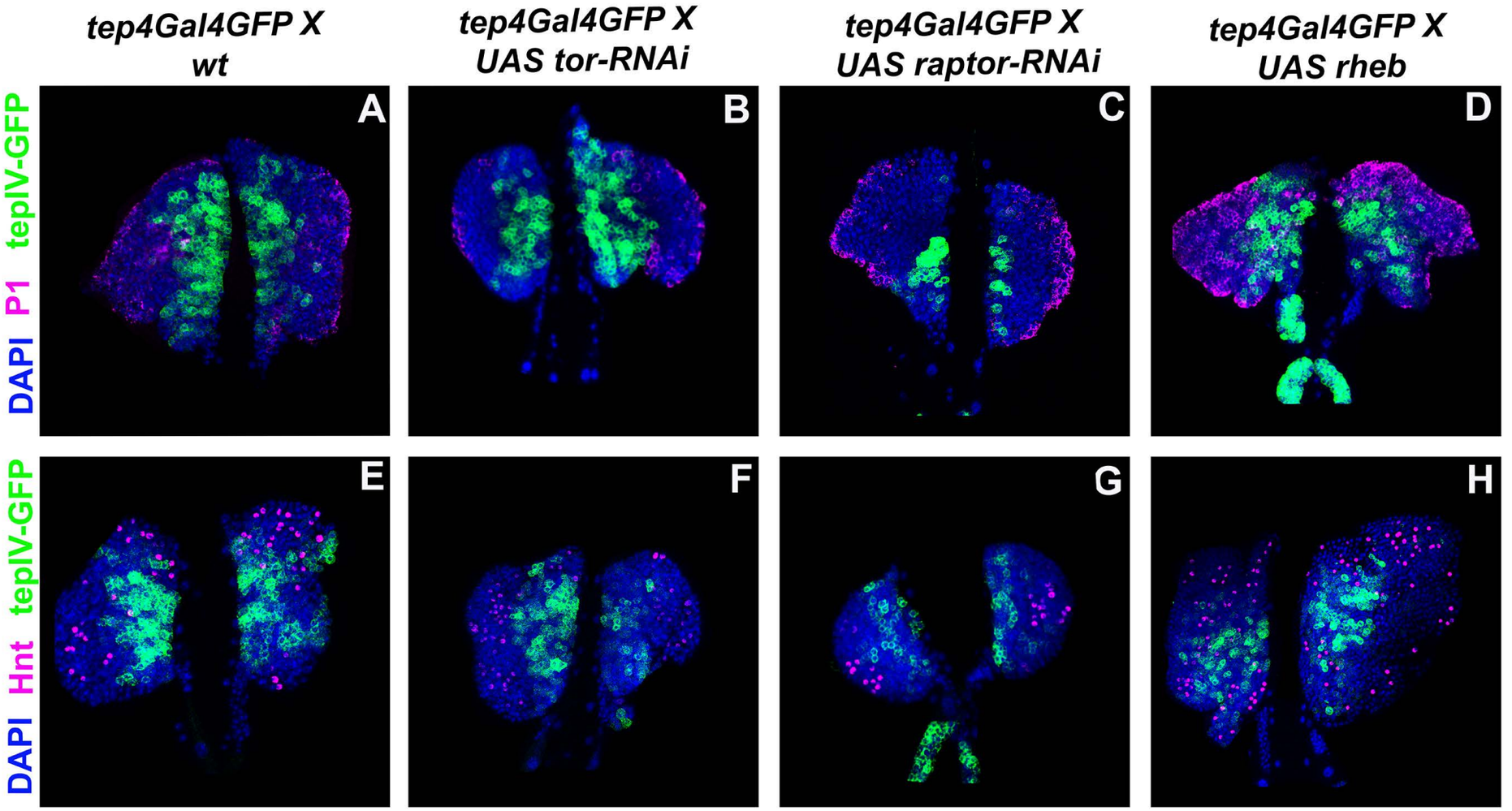
tep4Gal4GFP X wt
tep4Gal4GFP X UAS tor-RNAi
tep4Gal4GFP X UAS raptor-RNAi
tep4Gal4GFP X UAS rheb
tepIV-GFP
P1
DAPI
tepIV-GFP
Hnt
DAPI
A
B
C
D
E
F
G
H

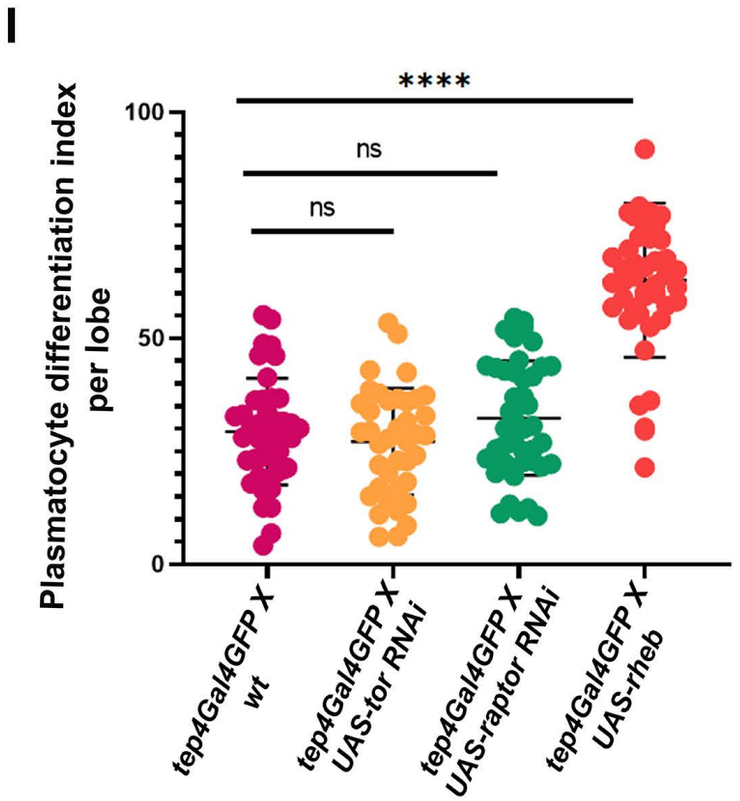
I
Plasmatocyte differentiation index per lobe
100
50
0
****
ns
ns
tep4Gal4GFP X wt
tep4Gal4GFP X UAS-tor RNAi
tep4Gal4GFP X UAS-raptor RNAi
tep4Gal4GFP X UAS-rheb

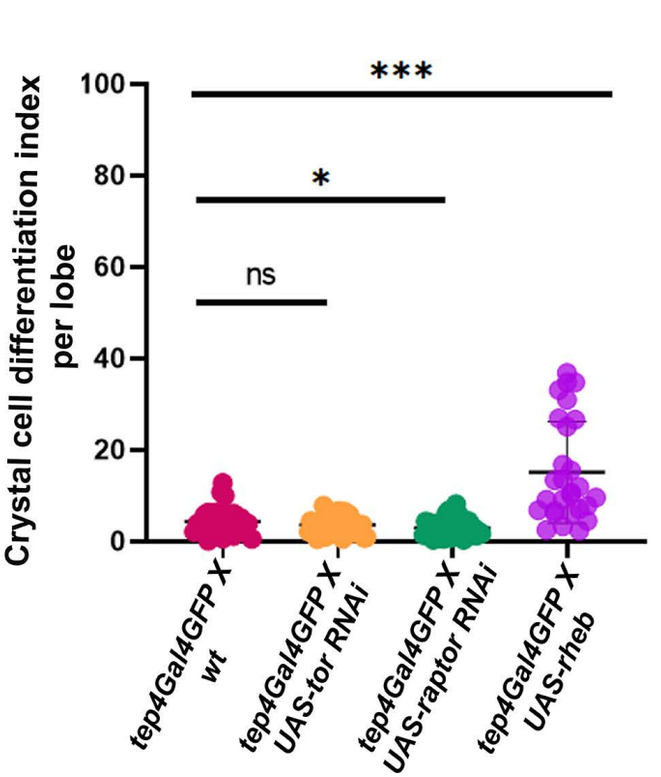
J
Crystal cell differentiation index per lobe
100
80
60
40
20
0
***
*
ns
tep4Gal4GFP X wt
tep4Gal4GFP X UAS-tor RNAi
tep4Gal4GFP X UAS-raptor RNAi
tep4Gal4GFP X UAS-rheb

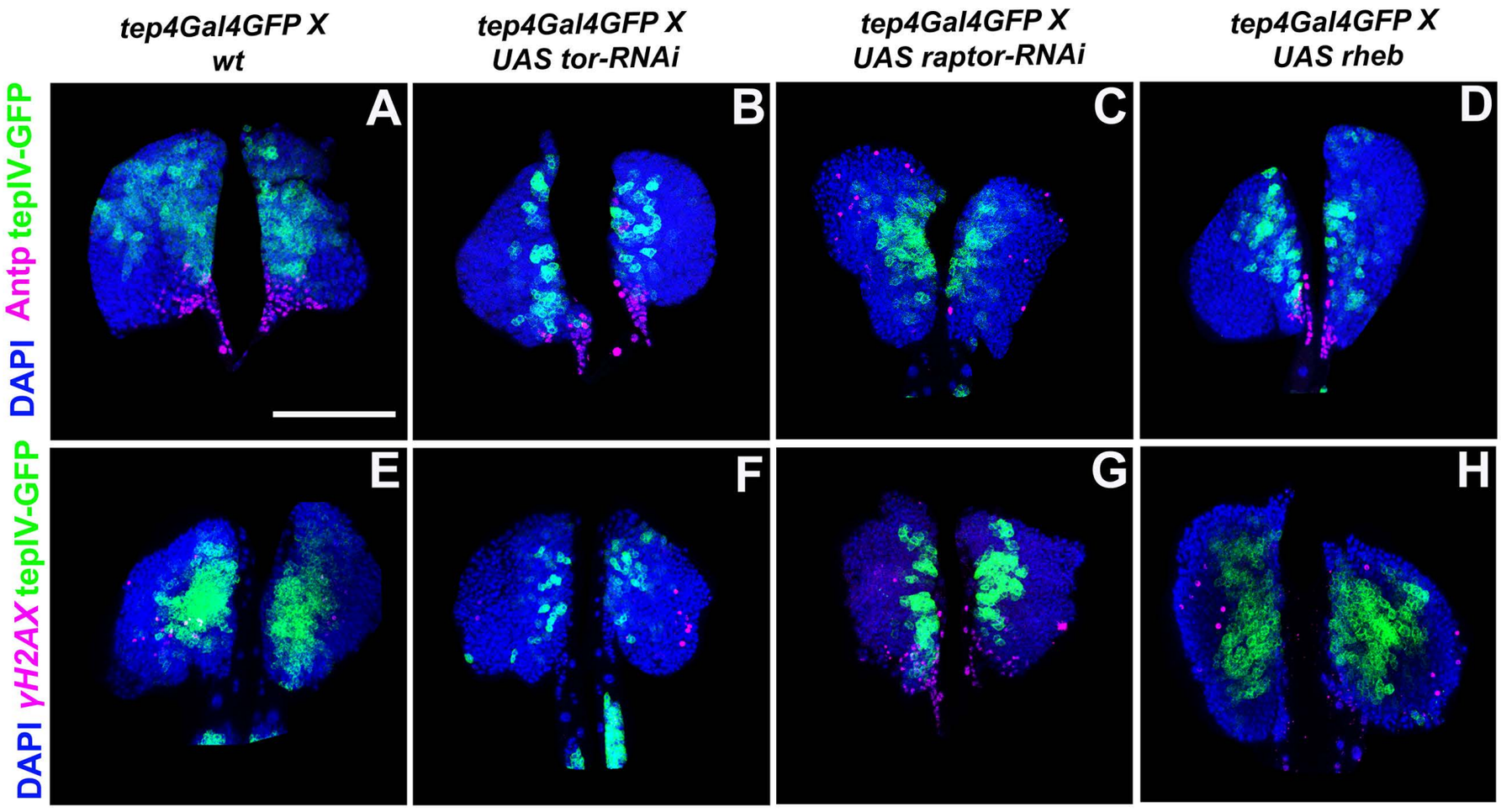
tep4Gal4GFP X wt
tep4Gal4GFP X UAS tor-RNAi
tep4Gal4GFP X UAS raptor-RNAi
tep4Gal4GFP X UAS rheb
DAPI Antp tepIV-GFP
DAPI γH2AX tepIV-GFP
A
B
C
D
E
F
G
H

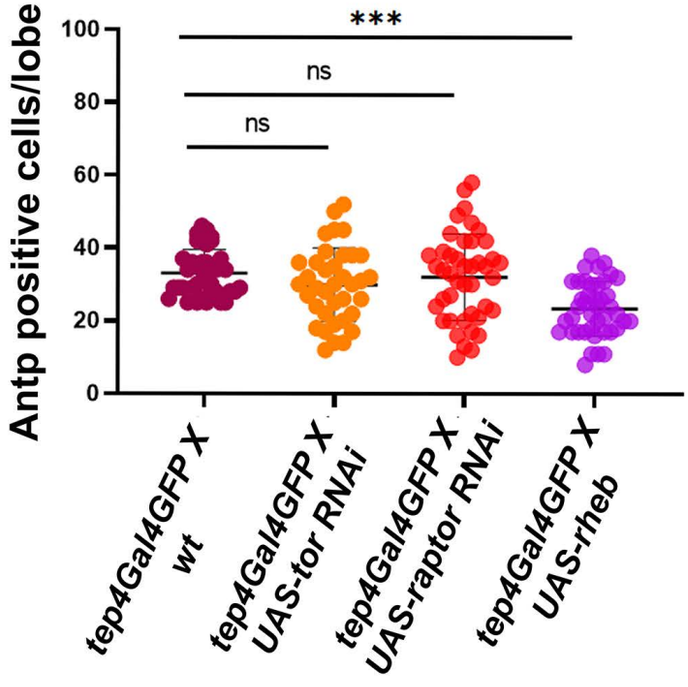
I
Antp positive cells/lobe
100
80
60
40
20
0
***
ns
ns
tep4Gal4GFP X wt
tep4Gal4GFP X UAS-tor RNAi
tep4Gal4GFP X UAS-raptor RNAi
tep4Gal4GFP X UAS-rheb

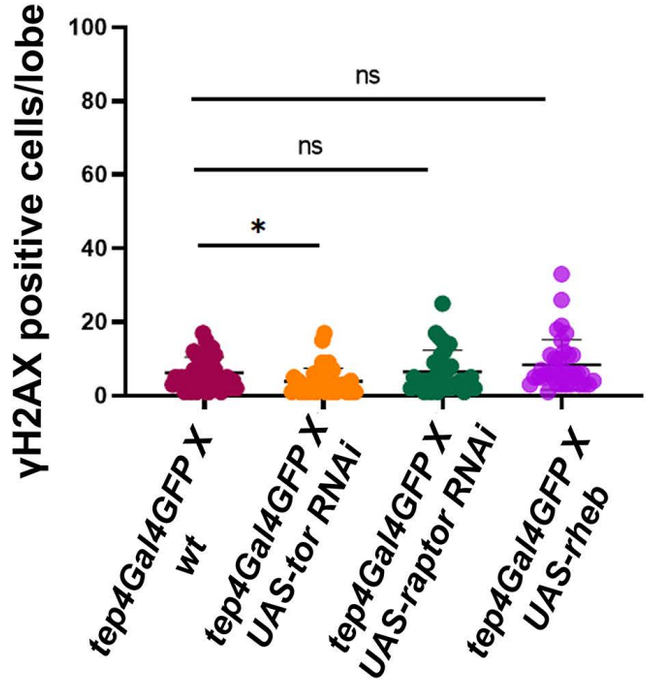
J
γH2AX positive cells/lobe
100
80
60
40
20
0
ns
ns
*
tep4Gal4GFP X wt
tep4Gal4GFP X UAS-tor RNAi
tep4Gal4GFP X UAS-raptor RNAi
tep4Gal4GFP X UAS-rheb